UNIVERSIDAD DE INVESTIGACIÓN DE TECNOLOGÍA EXPERIMENTAL YACHAY

Escuela de Ciencias de la Tierra, Energía y Ambiente

TÍTULO: PETROGRAPHIC STUDY OF THE PIMAMPIRO PLUTON, IMBABURA, ECUADOR

Trabajo de titulación presentado como requisito para la obtención del título de Geólogo

Autor:

Choez Macay Kewrin David

Tutor:

PhD. Vázquez Taset Yaniel Misael

Urcuquí, agosto de 2019

Urcuquí, 30 de agosto de 2019

SECRETARÍA GENERAL
(Vicerrectorado Académico/Cancillería)
ESCUELA DE CIENCIAS DE LA TIERRA, ENERGÍA Y AMBIENTE
CARRERA DE GEOLOGÍA
ACTA DE DEFENSA No. UITEY-GEO-2019-00003-AD

En la ciudad de San Miguel de Urcuquí, Provincia de Imbabura, a los 30 días del mes de agosto de 2019, a las 11:00 horas, en el Aula Al-101 de la Universidad de Investigación de Tecnología Experimental Yachay y ante el Tribunal Calificador, integrado por los docentes:

Presidente Tribunal de Defensa	Dr. ALMEIDA GONZALEZ RAFAEL VLADIMIR , Ph.D.
Miembro No Tutor	Dr. MARTIN MERINO, GERMAN , Ph.D.
Tutor	Dr. VAZQUEZ TASET, YANIEL MISAEL , Ph.D.

Se presenta el(la) señor(ita) estudiante CHOEZ MACAY, KEWRIN DAVID, con cédula de identidad No. 0929635506, de la ESCUELA DE CIENCIAS DE LA TIERRA, ENERGÍA Y AMBIENTE, de la Carrera de GEOLOGÍA, aprobada por el Consejo de Educación Superior (CES), mediante Resolución RPC-SE-10-No.031-2016, con el objeto de rendir la sustentación de su trabajo de titulación denominado: Petrographic study of the Pimampiro pluton, Imbabura, Ecuador., previa a la obtención del título de GEÓLOGO/A.

El citado trabajo de titulación, fue debidamente aprobado por el(los) docente(s):

Tutor	Dr. VAZQUEZ TASET, YANIEL MISAEL , Ph.D.

Y recibió las observaciones de los otros miembros del Tribunal Calificador, las mismas que han sido incorporadas por el(la) estudiante.

Previamente cumplidos los requisitos legales y reglamentarios, el trabajo de titulación fue sustentado por el(la) estudiante y examinado por los miembros del Tribunal Calificador. Escuchada la sustentación del trabajo de titulación, que integró la exposición de el(la) estudiante sobre el contenido de la misma y las preguntas formuladas por los miembros del Tribunal, se califica la sustentación del trabajo de titulación con las siguientes calificaciones:

Tipo	Docente	Calificación
Presidente Tribunal De Defensa	Dr. ALMEIDA GONZALEZ RAFAEL VLADIMIR , Ph.D.	9.4
Miembro Tribunal De Defensa	Dr. MARTIN MERINO, GERMAN , Ph.D.	9.9
Tutor	Dr. VAZQUEZ TASET, YANIEL MISAEL , Ph.D.	10.0

Lo que da un promedio de: 9.7 (Nueve punto Siete), sobre 10 (diez), equivalente a: APROBADO

Para constancia de lo actuado, firman los miembros del Tribunal Calificador, el/la estudiante y el/la secretario ad-hoc.

CHOEZ MACAY, KEWRIN DAVID
Estudiante

Dr. ALMEIDA GONZALEZ RAFAEL VLADIMIR , Ph.D.
Presidente Tribunal de Defensa

Dr. VAZQUEZ TASET, YANIEL MISAEL , Ph.D.
Tutor

Dr. MARTIN MERINO, GERMAN , Ph.D.
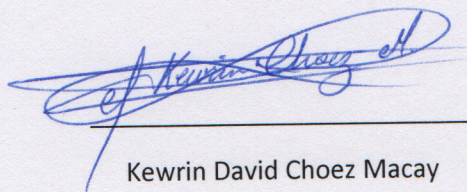Miembro No Tutor

TERÁN ROSALES, ANDREA YOLANDA
Secretario Ad-hoc

AUTORÍA

Yo, **KEWRIN DAVID CHOEZ MACAY**, con cédula de identidad 0929635506, declaro que las ideas, juicios, valoraciones, interpretaciones, consultas bibliográficas, definiciones y conceptualizaciones expuestas en el presente trabajo; así cómo, los procedimientos y herramientas utilizadas en la investigación, son de absoluta responsabilidad de el/la autora (a) del trabajo de integración curricular. Así mismo, me acojo a los reglamentos internos de la Universidad de Investigación de Tecnología Experimental Yachay.

Urcuquí, agosto de 2019.

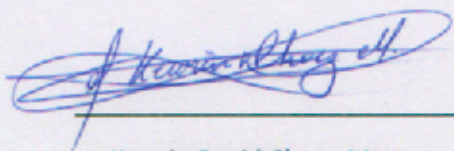Kewrin David Choez Macay

CI: 0929635506

AUTORIZACIÓN DE PUBLICACIÓN

Yo, **KEWRIN DAVID CHOEZ MACAY,** con cédula de identidad 0929635506, cedo a la Universidad de Tecnología Experimental Yachay, los derechos de publicación de la presente obra, sin que deba haber un reconocimiento económico por este concepto. Declaro además que el texto del presente trabajo de titulación no podrá ser cedido a ninguna empresa editorial para su publicación u otros fines, sin contar previamente con la autorización escrita de la Universidad.

Asimismo, autorizo a la Universidad que realice la digitalización y publicación de este trabajo de integración curricular en el repositorio virtual, de conformidad a lo dispuesto en el Art. 144 de la Ley Orgánica de Educación Superior

Urcuquí, agosto de 2019.

Kewrin David Choez Macay

CI: 0929635506

ACKNOWLEDGMENTS

INDEX

Abstract

     The Late Cretaceous evolution of the South American Margin is associated with subduction and accretion of oceanic lithosphere. The occurrence of I-type granitoids like the Pimampiro pluton during this epoch further suggest subduction beneath the South American Margin during the Late Cretaceous period. The petrography of the Pimampiro pluton and its mafic enclaves described in this work show that calcic amphibole megacrysts (> 30 mm) are dispersed on the pluton along with widespread phenocrystic hornblende (~ 1cm) and occasionally biotite as the major mafic mineralogy. Plagioclase feldspar in the pluton show anorthite contents that vary inside the andesine compositional field (An_{38}-An_{45}). Although previous studies have described the pluton as either a granodiorite (Litherland et al., 1994) or a hornblende-granodiorite (Chiaradia, 2013) our petrographic analysis determined a tonalite composition that along with the ubiquitous presence of hornblende in the pluton implies that it should be termed hornblende-tonalite under the IUGS systematics. The widespread hornblende minerals in the pluton place the Pimampiro tonalite on the Amphibole Calc-alkaline Granitoids (ACG) petrogenetic field of Barbarin (1999) which is consistent with subduction related origin during the Late Cretaceous, although geochemical analyses are needed to further confirm this hypothesis.

Keywords: Pimampiro, petrography, mineralogy, Cordillera Real, Imbabura.

Resumen

La evolución del margen suramericano en el Cretácico tardío está asociada con subducción y acreción de litósfera oceánica. La existencia de granitoides de tipo I como el plutón Pimampiro durante esta época sugieren subducción bajo el margen suramericano durante el periodo Cretácico tardío. La petrografía del plutón Pimampiro y sus enclaves máficos descritos en este trabajo muestran que los megacristales de anfíboles cálcicos (> 3 cm) están dispersos en el plutón junto con hornblenda fenocristalina (~ 1 cm) y ocasionalmente biotita como la principal mineralogía máfica. El feldespato de plagioclasa en el plutón muestra contenidos de anortita que varían dentro del campo de composición de andesina (An_{38}-An_{45}). Aunque estudios anteriores han descrito el plutón como una granodiorita (Litherland et al., 1994) o una granodiorita de hornblenda (Chiaradia, 2013), nuestro análisis petrográfico determinó una composición tonalítica que, sumado a la presencia ubicua de hornblenda en el pluton, este debería denominarse tonalita de hornblenda en base a la sistemática de la IUGS. Los minerales de hornblenda generalizados colocan la tonalita de plutón Pimampiro en el campo petrogenético ACG de Barbarin (1999), que es consistente con el origen relacionado con la subducción durante el Cretácico tardío, aunque se necesitan análisis geoquímicos para confirmar esta hipótesis.

Palabras clave: Pimampiro, petrografía, mineralogía, Cordillera Real, Imbabura.

1. Introduction

1.1   Introduction to the study area

The Pimampiro pluton is located on the eastern flank of the Cordillera Real in the northeast limit of the Imbabura UNESCO Global Geopark (Salazar et al., 1986; UNESCO, 2019). It is the oldest of a series of undeformed plutons intruding the Cordillera Real of Ecuador. Although outcrops are scarce in the Pimampiro region, it hosts a wide variety of igneous and metamorphic rocks of Paleozoic and Mesozoic age that record a long history about the formation of the Andes mountains of Ecuador (Litherland et al., 1994). The UNESCO designation brings the need of developing new geological research on the Imbabura province. Petrographic features can be observed at both macro and micro scales and can elucidate a broad history about the formation of the rocks in which they are found.

1.2   Background

Regional geochronological studies have identified twelve undeformed granitic intrusions of Late Cretaceous-Tertiary ages preserved along the Cordillera Real of Ecuador (Aspden et al., 1992a,b). These granitic bodies are associated with subduction of oceanic lithosphere beneath the South American plate. Among these, the Late-Cretaceous Pimampiro pluton shows megacrystic hornblendes that have not been described in other igneous rocks of the Ecuadorian Andes (Litherland, 1994). Published radiometric studies of the Pimampiro pluton have determined a wide range (Late Cretaceous to Middle Eocene) of K-Ar ages: 94 ± 4 Ma to 73 ± 2 Ma (Litherland, 1994). A zircon U-Pb age of 78.0 ± 1.2 Ma was published but not discussed by Cochrane (2013). The Pimampiro pluton is mapped in the San Gabriel geologic sheet (Salazar et al., 1986) and in the Geologic and Metal Occurrence Map (GMOM) of the Cordillera Real Metamorphic belt (Litherland et al., 1994) with marked differences regarding its rock name and limits.

1.3   Problem statement

The available geological maps of the Pimampiro pluton show marked differences regarding the limits of the pluton and the surrounding metamorphic units as well as the names employed to describe the rocks and the lithological units (Salazar et al., 1986; Litherland et al., 1994). This has brought confusion on the identification and location of these units in the northern portion of the Cordillera Real. Although some studies have been published for the vicinities of the Pimampiro pluton, most of them have been focused on determining the age of the rock units and thus the mineral paragenesis and the petrogenesis of the Pimampiro pluton remain uncertain. The lack of an appropriate petrographic description has brought uncertainties on the type of rock that makes up the pluton since only field names have been previously employed.

1.4   Objectives of the study

Present a detailed description of the mineral paragenesis and microtextures of the Pimampiro pluton and identify the rock type. Thin sections of the Pimampiro pluton and its host rock will be prepared and analyzed under a petrographic microscope for this purpose. The mineral paragenesis and the microtextures identified under the microscope will be used to retrieve information about the petrogenesis of the pluton. Finally, the modal percentages of appropriate mineral phases in both the pluton and its host rock will be employed to classify these rocks under the scheme of the IUGS Systematics of Igneous Rocks.

1.4.1   General objectives

a. Present macroscopic and microscopic descriptions of the textures and mineralogical composition of the igneous rocks found in the vicinities of the Pimampiro area.
b. Present a petrogenetic discussion about the origin of the pluton.
c. Classify these rocks from the Pimampiro pluton under the IUGS classification scheme and assign it a proper name.

1.4.2   Specific objectives

a. Compile the existing literature related to the study area.

b. Define the limits of the Pimampiro pluton and its metamorphic host rock from literature.

c. Identify the mineral species and the rock's microtexture under the petrographic microscope.

d. Calculate the modal percentages of the main mineral species.

e. Retrieve information about the process that affected the rock before and after its formation (i.e. diagenesis or metamorphism).

f. Classify the rocks and provide a name based on the recommendations of the IUGS Systematics of Igneous Rocks.

1.5   *General structure of the thesis*

The state of art of the geology and the geodynamic evolution of the Cordillera Real in relationship with the study area is presented in chapter two. Then, the methods employed to describe the main structures, textures and the mineralogical composition of the Pimampiro pluton and its host rock (chapter 4) are presented in chapter three. Chapter four compiles all the observations and the classification of the rocks under the IUGS scheme. These observations are finally interpreted, discussed and summarized in chapter five.

2. *Theoretical background*

Whilst the aim of this project is to provide a petrographic description of the Pimampiro pluton, it has been proven that the petrographic characteristics of granitoid are strongly influenced by the geodynamic environment in which they form (Barbarin, 1990). Therefore, the basement of the area surrounding the Pimampiro pluton and the geodynamic models available for the formation of the Cordillera Real will be described on the next subchapters as means for understanding the geologic history and the particular setting that prevailed on the South American Margin (SAM) at the time of formation and crystallization of the Pimampiro pluton.

The closure temperature is the temperature at which certain mineral phase begins to accumulate daughter isotopes of a determined radiogenic system (i.e. Ar/Ar, U-Pb, K/Ar, Rb/Sr) without loses from the crystal by thermally activated diffusion (DiPietro, 2013; Harrison 1982). Below this temperature, the crystals have a closed system behavior and

thus their concentrations of isotopes record the real age of that mineral. Zircons have very high closure temperature (> 900 °C) in the U-Pb system (Cherniak & Watson, 2001). The hornblende minerals have high closure temperature (500 ± 25 °C) in the ^{40}Ar/^{39}Ar system compared to muscovite (425 ± 25 °C) and biotite (330 ± 25 °C) minerals. These temperature ranges vary from model to model, depending on grain size, diffusion radii and cooling rate (Harrison, 1982) but in general the high thermal stability of zircons make possible the retrieval of true crystallization ages. The ^{40}Ar/^{39}Ar system ages obtained from hornblende, biotite or muscovite minerals must be approached with care because the relatively low closure temperature of these minerals which makes them susceptible to thermal diffusion and thus resetting of the ages due to younger thermal events such as magmatism or metamorphism (Harrison, 1982). Based on the previous discussion, the Campanian zircon age (78.0 ± 1.2 Ma) presented by Cochrane (2013) is the most reliable crystallization age available for the Pimampiro pluton and therefore will be considered to discuss the geological framework at the type of its formation.

2.1 Geological framework

The Ecuadorian Andes comprise two subparallel mountain ridges trending NNE-SSW: the older Cordillera Real or Eastern Cordillera, and the younger Cordillera Occidental (CO) or Western Cordillera (Aspden & Litherland, 1992; Fig. 1). Between these two mountain ranges there is the Inter Andean Depression (IAD), a graben covered by Plio-Pleistocene volcanic deposits on top of which the largest cities of the Ecuadorian Andes are settled. The Inter Andean depression is limited to the west by the Calacalí-Pallatanga-Palenque fault and to the east by the Peltetec fault. The western margin of the Cordillera Real is the Baños fault which separates oceanic rocks (i.e. Alao-Paute unit) in the west from continental derived series (i.e. Sabanilla unit) in the east. The Cosanga, Mendez and Palanda faults define the western limit of the South American craton in Ecuador, separating unmetamorphosed rocks on the east (Sub Andean Zone) from the metamorphic rocks of the Cordillera Real on the west.
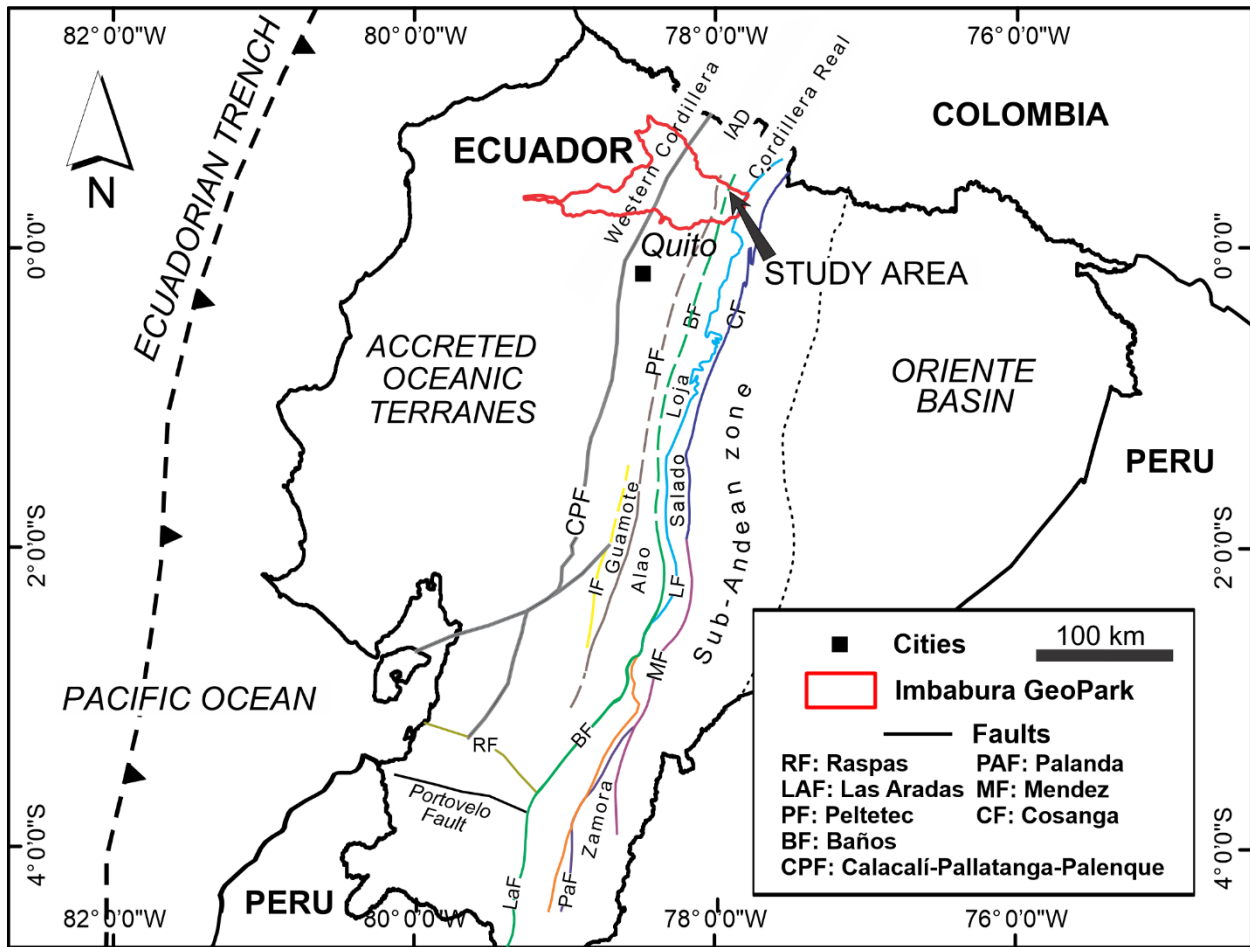
Figure 1. Schematic structural map of the Ecuadorian Andes: principal faults, geomorphological terranes, and metamorphic divisions of the Cordillera Real are labeled. Modified after (Aspden & Litherland, 1992; Litherland et al., 1994). IAD: Inter Andean Depression.

Based on an allochthonous model for the evolution of the South American Margin, the Cordillera Real was divided into five tectonostratigraphic terranes: Guamote, Alao, Loja, Salado and Zamora (Litherland, 1994). These divisions comprise a wide variety of metaigneous, metamorphic and meta-sedimentary units whose ages span from Paleozoic to Mesozoic times. Although the autochthonous model for the geodynamic evolution of the SAM proposed by Pratt et al. (2005) is currently the most accepted model, the divisions made by Litherland et al. (1994) remain mostly unchanged. According to the available geologic maps, the basement surrounding the Pimampiro pluton may involve three out of the five divisions of the Cordillera Real (Guamote, Alao and Loja) proposed by Litherland et al. (1994). These divisions will be described further in

this section (subsections 2.1 - 2.3) and summarized from literature (subsection 2.4) as means for understanding the geologic setting and history of the area surrounding the Pimampiro pluton in a regional context. The geologic history of the area will be partially used to contrast or support the petrogenetic discussion on the link between the resulting petrographic features and the prevailing geodynamic environment that induced the formation of the Pimampiro pluton.

2.1.1 The metamorphic basement

2.1.1.1 Loja terrane

During the late Triassic the semi-pelitic sediments from the Loja terrane were metamorphosed along the eastern Andes of Ecuador. This event is associated with the emplacement of syn- to post-tectonic S- and I-type granitoid batholiths, amphibolite bodies and migmatite formation (Egüez & Aspden, 1993; Litherland, 1994). The Loja terrane contains the oldest rocks from the Cordillera Real. East of the Baños fault this division is represented by the Tres Lagunas unit, a belt of S-type plutons that extend all along the Cordillera Real (Aspden et al., 1992b). Similarly, associated migmatites and metamorphic semi-pelitic to psammitic rocks from the Sabanilla, Chigüinda and Agoyán units, and the Monte Olivo amphibolites, were assigned to this terrane by Aspden & Litherland (1992). The western limit of this terrane is the Baños fault and its southern continuation, the Las Aradas faults (Aspden et al., 1992a). The rocks of the Loja terrane are characterized by near-vertical (70-80°) west-dipping Andean-trending second schistosity.

The minimum alteration age for the Tres Lagunas unit is poorly constrained by Rb-Sr dating to 200 ± 12 Ma (MSWD=169.1) due to a high degree of scatter (Aspden et al., 1992b). Younger K-Ar ages ranging from 100 ± 3 Ma to 51 ± 2 Ma from the Tres Lagunas granite at three different locations along the Cordillera Real are interpreted as reset ages due to Cretaceous accretionary episodes (Aspden et al., 1992a,b). K-Ar ages from muscovite from similar rocks adjacent to the Tres Lagunas granite yield Late Cretaceous (74 ± 3 Ma) age (Aspden & Litherland, 1992). The high initial $^{87}Sr/^{86}Sr$ ratio (i.e. 0.7120) of the Tres Lagunas unit suggests that high crustal contamination occurred during the formation of the granitoid. The Tres Lagunas granite was classified as S-type granitoid by Aspden et al. (1992a) and has characteristic smorky-blue quartz.

The Sabanilla unit is the high-grade country rock of the Tres Lagunas unit. It comprises mainly foliated and partly migmatitic biotite ± garnet ± muscovite-bearing orthogneisses (metaigneous) and migmatites (Aspden & Litherland, 1992). Associated metasedimentary rocks usually contain garnet and staurolite; sillimanite and kyanite are also present. Amphibolite intrusions made of hornblende + plagioclase ± biotite have been reported as being common within the metaplutons. The origin of the granitoids within the Sabanilla unit is controversial but is clearly distinct from the Tres Lagunas unit due to higher 87Sr/86Sr ratios, absence of alkali feldspars megacrysts and blue quartz (Aspden et al., 1992a). K-Ar dating of para- and ortho-gneisses from this unit at the Zamora province yield Late Cretaceous ages that range between 85 ± 2 and 65 ± 2 Ma which correspond to reset ages associated with Cretaceous accretionary episodes (Aspden & Litherland, 1992).

The Chigüinda unit comprises a sequence of quartzites of fine to medium grain size, metamorphic siltstone, graphitic schist, phyllite, slate and metagraywackes. Palynological studies have revealed post-Silurian depositional ages in the Loja-Zamora region (Litherland et al., 1994). Chew et al. (2007) reported an age of 362 ± 12 Ma for the youngest detrital zircon of the Chigüinda unit in the Loja province. The most probable environment for the deposition of this unit is either an intracratonic basin or a passive margin with contributions of continental material. The Agoyán unit replaces the Chigüinda unit in the northern portion of the Cordillera Real. It is considered the high-grade equivalent of the Chigüinda unit and consists of coarse-grained gneisses, garnet-bearing (up to 1 cm across) micaceous schists and metapsammites (Litherland, 1994).

The Monte Olivo unit comprises all the tholeiitic basalts (i.e. amphibolites) in the Loja terrane. The unit was named after the Monte Olivo town where it was first described. The rocks forming this unit represent a phase of mafic dikes and sills cutting the Chigüinda-Agoyán metasediments along the Late Triassic paleo-margin of Ecuador in a rift environment (Cochrane, 2013). It includes amphibolite schists and amphibolite of Back Arc Basin Basalt (BABB) and Normal Mid Ocean Ridge Basalt (N-MORB) affinity. The amphibolites of BAAB affinity were gradually replaced by primitive N-MORB amphibolite dikes as the back-arc basin on northwestern South America evolved into a rift during the Triassic (Cochrane, 2013). Far south in the Loja province area, the rocks from this unit feature a high grade of weathering and transitional contacts with the host rock. Chlorite schists are altered to biotitic schists, phyllites and quartzites.
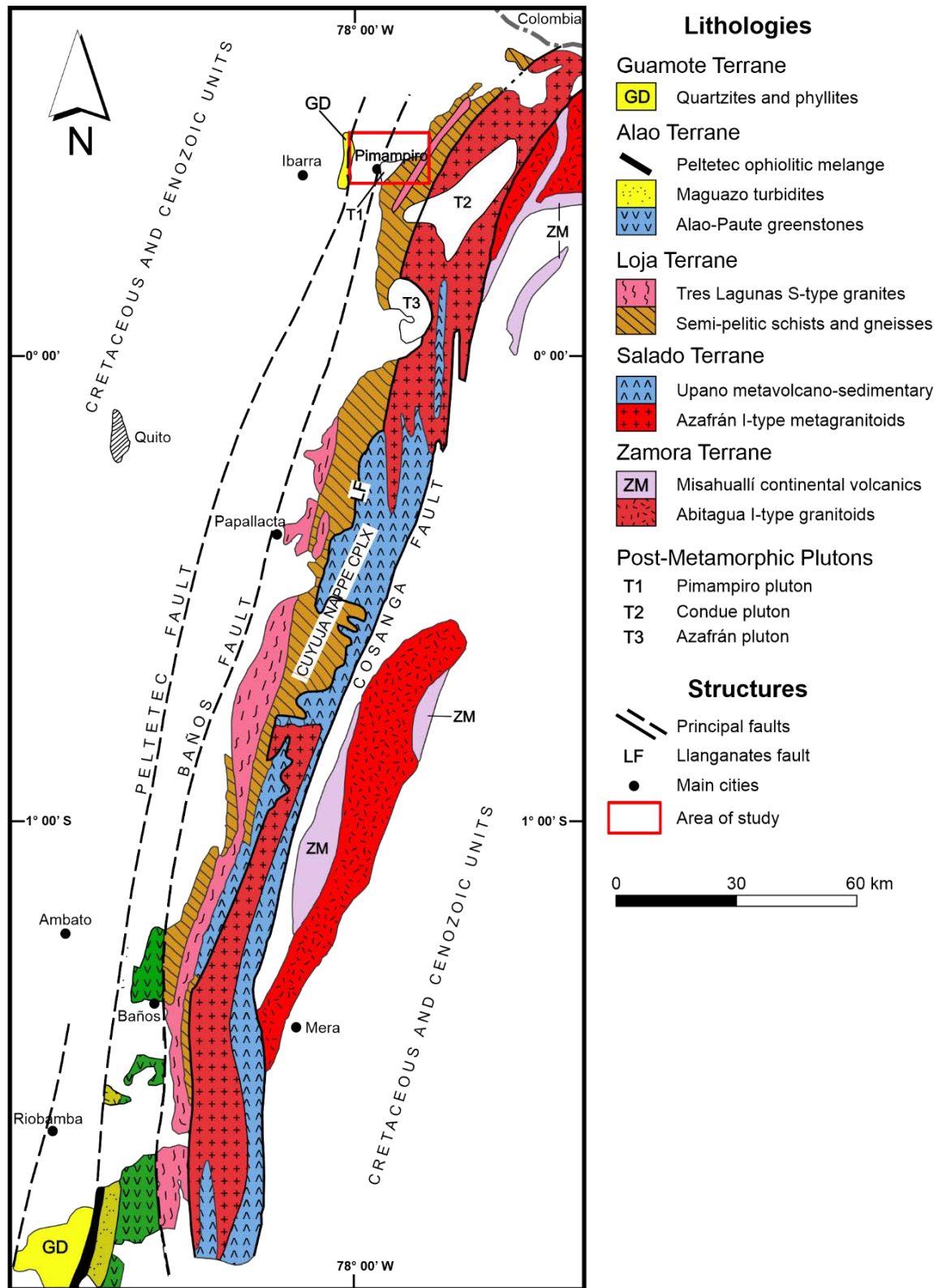
Figure 2. Location and simplified geological map of the Cordillera Real between the Colombian border and the city of Riobamba modified from (Aspden et al, 1992a, 1992b; Litherland, 1994).

2.1.1.2 Alao terrane

The beginning of slab roll-back at 145 Ma on the east-subducting proto-Pacific plate caused calk-alkaline and tholeiitic arc magmatism, occasionally Transitional-MORB basalts, and the deposition of marine sedimentary units until 141 Ma on the Cordillera Real (Litherland et al., 1994; Spikings et al, 2015). The protracted westward migration of the volcanic arc generated the Azafrán batholith and the younger Alao arc (Spikings et al., 2015). The Alao terrane is a ~30 km-wide belt of variable metavolcanics and metasedimentary rocks (Aspden & Litherland, 1992). It comprises the Peltetec, Alao-Paute, El Pan and Maguazo units. The Peltetec fault is the western limit of the terrane (Fig. 2). The Baños fault divides the Paleozoic-Triassic high-grade units of the Loja terrane from the rocks of the Alao terrane (Aspden & Litherland, 1992). Outcrops of the Alao terrane have been reported along the western flank of the Cordillera Real mainly between Ambato and Cuenca and although the Baños fault has been proposed to extend further north towards Ambuquí and Pimampiro, outcrops of the Alao division have not been reported in the area.

The Peltetec fault separates the continent-derived Guamote terrane from the oceanic turbidites of the Maguazo unit in the Alao terrane (Aspden & Litherland, 1992). The Peltetec unit outcrops along the Peltetec fault. It consists of remnants of an obducted ophiolite sequence deformed by a series of Andean-trending near-vertical shear zones (Aspden & Litherland, 1992). The Peltetec unit comprises a narrow (< 2km) series of outcrops that include cherts and phyllites, basalts, dolerites, serpentinites, gabbro, peridotite and minor tectonic lenses of the Tres Lagunas granite (Aspden & Litherland, 1992). The presence of this ophiolitic mélange along with volcanic rich turbidites from the Maguazo unit and the absence of similar or equivalent rocks east of the Alao-Paute greenstones (meta-andesites) is in agreement with the interpretation of the Peltetec fault as a former subduction zone (Spikings et al., 2015).

The Maguazo unit is mainly formed by andesitic greenstones and turbidites of Callovian-Oxfordian Jurassic age (Aspden & Litherland, 1992). Other lithologies such as metamorphosed tuffs, carbonaceous slates, marbles, orthoquartzites and cherts are also included in this unit. The Alao-Paute unit is immediately west of the Baños fault at the town of Baños and is mainly constituted of andesitic greenstones and greenschists. The greenstones and greenschists of the Alao-Paute unit commonly show widespread chlorite ± albite ± quartz ± epidote ± biotite ± actinolite mineralogy, characteristic of greenschist facies (Aspden & Litherland, 1992). It is not clear if these rocks were formed in a marginal or oceanic basin setting (Aspden & Litherland, 1992).

The Baños fault is the present western limit of the Cordillera Real and the eastern limit of the Alao terrane. It marks a lithological and metamorphic grade change. This fault can be traced between Pimampiro (inferred) in the north and Saraguro in the south where it continues as the Las Aradas fault. The extension of this fault north of Pimampiro into Colombia is correlated with the Romeral fault zone (Aspden et al., 1992a), an extinct subduction zone (Chicangana, 2005). The Baños fault marks the easternmost occurrence of pelitic schists, gneisses and metagranites from the Loja terrane (Aspden & Litherland, 1992). Sigmoidal quartz eyes are indicative of dextral movement along the Baños fault (Litherland, 1994) but recent studies link the absence of vertical displacement along the Baños fault with an intrusive nature (Pratt et al., 2002; Spikings et al., 2005) rather than the former tectonic nature proposed by (Litherland et al., 1994) in accordance with the autochthonous model for the evolution of the Cordillera Real proposed by Pratt et al. (2005).

2.1.1.3 Guamote terrane

The Guamote terrane consists of lower Jurassic to lower Cretaceous epicontinental clastic (marine) metasediments (Litherland et al., 1994). The units of the Guamote terrane were deposited on the passive margin of the allochthonous Chaucha plate of Litherland (1994). In broad terms, this terrane comprises continentally-derived orthoquartzites intercalated with low-grade phyllites or slates (Spikings et al., 2015) and is divided into three units: Cebadas, Guasuntos and Punín according to their relative content of quartzite and phyllite. Clastic blue quartz probably derived from the Tres Lagunas granite along with undeformed acid volcaniclasts are present within the sediments of the Guamote terrane (Litherland, 1994). It outcrops along the western margin of the Cordillera Real, mainly between Riobamba and Azogues but similar lithologies outcrop as "inliers" near Ambuquí (Litherland, 1994). The Chaucha-Arenillas gneissic terrane is thought to be present at depth west of the Peltetec fault and is thought to have sourced the Guamote terrane during Mesozoic time as the closure of the Alao ocean/marginal basin occurred. Zircon U-Pb data from allochthonous Late Cretaceous rocks show that the crystalline basement located to the west of the Peltetec fault form part of the Caribbean plate (Spikings et al., 2011).

2.1.2 Post-deformational magmatism in the Cordillera Real

Most of post-deformational plutons in the Cordillera Real are dated between 80 and 40 Ma (Aspden et al., 1992b). These relatively small plutons were emplaced due to episodic events during Cretaceous-Paleocene (ca. 73-60 Ma) to Early Tertiary (ca. 60-38 Ma) time (Egüez & Aspden (1993). According to K-Ar data from Aspden et al. (1992b) the oldest undeformed pluton in the Cordillera Real is the Pimampiro pluton (94 – 73 Ma) and the youngest is the Portachuela pluton (24 – 12 Ma; K-Ar). These ages are interpreted as magmatic cooling ages by Aspden et al. (1992b). The Condue and Azuela plutons were not dated in their study but are inferred to be Tertiary due to lack of deformation in concordance with other similar plutons (Aspden et al., 1992b).

There are 2 peak events of reset mineral ages recorded in the Cordillera Real during the Cretaceous period (Aspden et al., 1992b). The Cretaceous resetting of the K-Ar ages is related to thermal events. The earliest resetting occurred during the Early Cretaceous (ca. 135 – 125 Ma) and the second occurred during the Late Cretaceous period (ca. 85 – 65 Ma). The K-Ar mineral age disturbances during the Late cretaceous are related to the uplift of the Cordillera Real according to (J. A. Aspden, Harrison, et al., 1992b). These peak events will be considered for the discussion of the geological history of the terranes from the Cordillera Real.

2.1.3 Geodynamic evolution of the Cordillera Real

The main events associated with the geodynamic evolution of Ecuador that occurred during the Triassic, Jurassic and Cretaceous periods are described by Egüez & Aspden (1993). Vestiges of the disassembly of western Pangaea along the Andes of Ecuador are hosted within the Cordillera Real. Three major phases can be distinguished along the Cordillera Real of Ecuador during late Permian-Late Jurassic epochs: the pre-rifting phase, the rifting phase and the southeastward subduction (Jaillard et al., 1995). The Triassic rifting along western Pangea is thought to be recorded in the lithologies from the Loja terrane. Crustal anatectites in Ecuador include the massive granites from the Tres Lagunas unit and the associated Sabanilla migmatites and Monte Olivo amphibolites (Cochrane et al., 2014b). According to Cochrane et al. (2012) magmatism, terrane collision and accretion events dominated the evolution of the Cordillera Real since the Early Jurassic.

The two main hypotheses proposed for the Late Paleozoic - Early Triassic plate evolution of the southwestern Tethyan system differ in whether the present-day Mexican and Central American continental blocks were in front of the presently Venezuelan or Colombian margins (Jaillard et al., 1995). In the former case the NNE-trending Colombian segment should have been facing the subduction of the paleo-Pacific since the late Paleozoic Era. On the other hand, possible subduction of the paleo Pacific plate must have occurred beneath the Mexican and Central American blocks (continental microplates) and subduction facing the Colombian segment could only have occurred after these continental microplates were pushed apart from the South American Plate. The ambiguities regarding these two hypotheses arise from uncertainties on the origin of the displaced terranes of Central and North Andean regions. Jaillard et al. (1995) present the geodynamic relations between the Andean and Tethyan realms between Late Permian and Late Eocene time. During the Mesozoic Era the Andean Cordillera of northwestern South America can be divided in two segments: the NNE-trending Colombian segment which includes most of Colombia and Ecuador and the NW-trending Peruvian segment (Jaillard et al., 1995). Currently, the NNE-trending segment comprises an axial cordillera cored by Paleozoic to Mesozoic metamorphic rocks (Cordillera Oriental of Colombia and Cordillera Real of Ecuador).

Based on a summary of the relevant sedimentary, tectonic and magmatic events recorded in the Central and North Andean margins Jaillard et al. (1995) conclude that: a) the influence of the Tethyan system on the evolution of the Andes has diminished significantly since the Triassic epoch, b) during the Middle Jurassic epoch South America remained stable at its position and that spreading of the NE-trending Tethyan ridges was the main control for the Andean subduction during this time, c) the convergence became mainly directed towards the NE as Tethyan spreading centers die out during early Late Cretaceous epoch, and d) opening of the equatorial South Atlantic Ocean induced the westward motion of South America and a change in converge direction to ENE during Eocene epoch, e) the opening of the Indian Ocean drove the "northward shift of the Gondwanian plates and the beginning of the reabsorption of the Tethyan ocean" (Jaillard et al., 1995). Tethyan-controlled southwestward convergence enabled the onset of a magmatic arc on the Colombian segment but the development of a dextral transform boundary outboard the Peruvian border during the Middle Jurassic epoch (Jaillard et al., 1995). The shift on the convergence direction to NE during the early Late Cretaceous epoch induced the formation of a magmatic arc on the Peruvian segment and a dextral transform boundary on the Colombian segment. Finally,

15

during the Eocene epoch the westward shift of South America caused compressive deformation and arc magmatism along the entire Andean margin. Change in paleo Pacific plate motion from NNE to ENE direction provoked terrane accretion (island-arc collisions) during Paleocene-Eocene time along the former transform boundary of the Colombian segment. From then on, the tectonic evolution of the Andean margin has been controlled by the nearly orthogonal convergence of the Pacific plate which has caused typical forearc-arc-foreland zonation (Jaillard et al., 1995).

Rifting along western Pangaea started with the opening of a back-arc basin behind a Permian arc. The beginning of rifting within western Pangaea at 240 Ma induced seafloor spreading between Central and South American blocks and the formation of oceanic crust at ~216 Ma (Cochrane, 2013; Spikings et al., 2015). The transition from rift to drift and onset of seafloor spreading occurred during 225–216 (Cochrane et al., 2014b). According to Litherland et al. (1994), the northwestern South American Margin became active at ~209 Ma due to the east-dipping subduction of the Farallon oceanic lithosphere (proto-Pacific plate). This event is recorded by the occurrence of metaluminous, I-type arc rocks along northwestern South America as old as 209 Ma. According to Cochrane et al. (2014b) the subduction of the proto-Pacific plate beneath northwestern South America started between ~213, ~190 and ~185 Ma in Venezuela, Colombia and Ecuador Andes respectively. Spikings et al. (2011) reported Early Jurassic ages (~183Ma; U-Pb from zircons) for the beginning of the active margin arc magmatism along northwestern South America. This Jurassic arc remained active until ~143 Ma when the introduction of buoyant seamounts into the subduction zone caused rapid oceanward migration of the trench. The opening of the South Atlantic Ocean drove South America westward causing a change from extension to compression of the South American Pacific margin at 120-110 Ma. This led to the closure of the back-arc basin and caused its obduction onto the continental margin of South America (Peltetec unit in Ecuador) during 117-107 Ma (Spikings et al., 2011). The subduction resumed further west. The collision and accretion of oceanic plateau (possibly the Caribbean Oceanic Province) at 75 Ma ceased passive margin conditions (Spikings et al., 2015). The motion direction change of the paleo-Pacific plate from likely NNE to ENE provoked terrain accretion and marked tectonic events on the Andes during Late Paleocene-Eocene time (Jaillard et al., 1995).

According to the geodynamic evolution model of Kerr et al. (2002, 2005), the SAM experienced several periods of terrane accretion during the Late Cretaceous to Eocene time. Protracted accretionary events during the Late Cretaceous were originated by the collision of the Pallatanga oceanic plateau with the SAM after subduction of the associated thin oceanic crust along the east-dipping subduction zone (Fig. 3). This is the most probable geodynamic environment prevailing at the time of formation of the Pimampiro pluton. Extensive discussion on the geodynamic evolution of the SAM during the Late Cretaceous is provided by Kerr et al. (2002, 2005) and Vallejo et al. (2019).
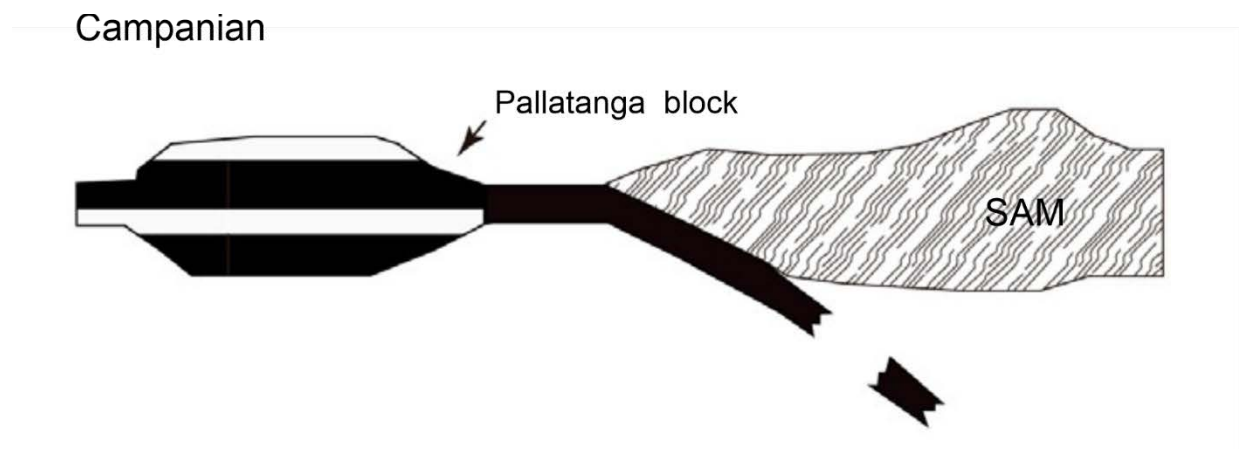
Figure 3. Oversimplified schematic diagram of the plate dynamics across the SAM during the Campanian. Subduction-related subalkaline arc magmatism is not shown but is generally agreed in these type of environments (Barbarin, 1990). Diagram reproduced after Kerr et al. (2002).
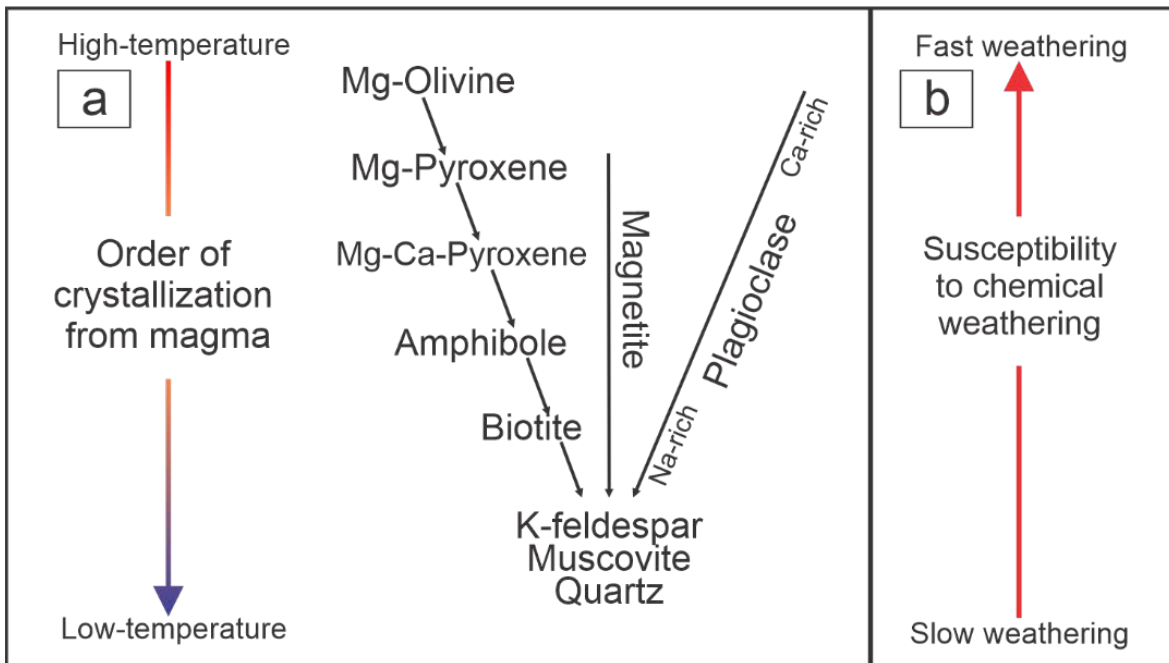
2.2   *Petrogenesis of igneous rocks*

Interpreting the microstructures of plutonic and metamorphic rocks requires a previous understanding of the crystallization process of minerals (Vernon, 2004). Igneous minerals are characterized for their crystallization out of a melted body upon cooling in contraposition to solid-state growth of metamorphic minerals (Vernon, 2004). For crystallization of an igneous mineral to occur, an embryo or seed must first form (nucleate). This embryo must be thermodynamically stable, meaning that melt must achieve certain amount of cooling so that more atoms can attach to viable nuclei allowing it to growth into a crystal (Vernon, 2004). The interplay between nucleation rate and growth rate determines the crystal size distribution (CSD) of minerals in igneous rocks (Marsh, 1988; Vernon 2004).

The color index of igneous rocks is associated with the amount of light (i.e. felsic) versus dark (i.e. ferromagnesian) minerals. It is a measure of the ratio between the amount (%) of dark (mafic) and light (felsic) colored minerals. An igneous rock with high color index contains higher proportions of mafic minerals than a rock with low color index. Thus, the color index may be a good indicator of the mafic affinity of a magmatic system. In granitic rocks, the high color indexes of mafic enclaves reflect their higher mafic composition in comparison to the usually more evolved host rocks with lower color indexes (Vernon, 2004).

2.2.1   *Bowen reaction series and Goldich weathering sequence*

The Bowen reaction series describe how minerals change as they crystallize out of magma (Bowen, 1922). It ranks silicate minerals based on the temperature at which they crystallize. This idealized progression in which minerals crystallize out of magma upon cooling presented by Bowen (1922) is still accepted as the general model for the evolution of subalkaline magmas through fractional crystallization. His experimental results on the order of crystallization of the common silicate minerals are presented as two reaction series (Fig. 4). The scheme is composed by a discontinuous series of ferro-magnesian minerals (left arm in Fig. 4) and a continuous series of calcium-sodium feldspars (right arm in Fig. 4). The discontinuous series involves the destruction of partial reaction of previously formed high-temperature minerals with the magma to produce lower-temperature phases. Contrastingly, the continuous series do not necessarily involves the destruction of high-temperature plagioclase (An-rich) to form low temperature varieties (Ab-rich) because there is complete solid solution in the plagioclase feldspars, thus the precipitation of sodium-rich plagioclase occurs gradually on top of the calcium-rich plagioclase (normal zoning) as the surrounding melt evolves into a more felsic composition through fractional crystallization (Bowen, 1922). It is noteworthy that all minerals in the discontinuous series are Fe-bearing minerals, and some of them are water-bearing. If oxygen pressure is high enough during fractional crystallization, magnetite can co-precipitate with phases of the Bowen series (Osborn, 1962). The diachronous precipitation of magnetite reduces the overall concentration of the mafic components of the melt, particularly the Fe-concentration. This co-precipitation coincides and justifies the slightly decrease of Fe-concentration observed at different stages during the evolution of calc-alkaline magma suites (Osborn, 1962).

Inversely analogous to the Bowen reaction series, the Goldich dissolution series (indicated by the red arrow in Fig. 4) is a way of predicting the stability to chemical weathering (weathering rate) for minerals exposed to Earth's surface conditions (Goldich, 1938). Based on soil profiles analyses, Goldich (1938) demonstrated that minerals formed at high temperatures and pressures are less stable to surface conditions than minerals formed at lower temperatures and pressures. This relationship is based on the proportion of covalent bonds versus ionic bonds in silicate minerals. The atoms in minerals with high proportions of silica (high silica polymerization) are bounded mainly by covalent bonds (i.e. tectosilicates) while minerals with low polymerization (i.e. nesosilicates) have a greater amount of ionic bonds due to greater proportion of ions in the mineral structure (Goldich, 1938). This implies that minerals that crystallize first (e.g. calcic plagioclase) undergo greater amounts of chemical weathering than the late phases (e.g. sodic plagioclase).

Figure 4. a) Bowen reaction series (black and red-blue arrows) and b) Goldich weathering sequence (red).

2.2.2 Common microstructures of igneous rocks

Twinning is a common feature observed in minerals under the petrographic microscope (Neese, 1986). Twinning can be defined as the jointing between two or more crystals of the same substance following a symmetry law (Demange, 2012; pg. 37). Simple, contact, polysynthetic, cyclic and penetration twins are the most common types. Carlsbad twinning is a type of penetration twinning with [001] as the twin axis (Nesse, 1986). Carlsbad twinning preferentially occurs in feldspars of intermediate composition in comparison with polysynthetic twinning that is more common in plagioclase feldspars (Nesse, 1986). The occurrence of cross-hatched twinning in plagioclase is limited to a few cross twins per grain in comparison to the complex tartan texture developed by K-rich feldspars (i.e. microcline), thus distinction between these types of feldspars can be made by means of microscopic examination (Nesse, 1986).

Feldspars are the most common mineral on Earth's crust. Feldspars are aluminosilicates minerals with triclinic and monoclinic symmetries (Nesse, 1986). Their structure is a three-dimensional framework composed by corner-bounded SiO_4 and AlO_4 tetrahedra (tectosilicate) and interstitial cations (Ba^+, Na^+, K^+, Ca^{2+}). Small or heavily charged cations (i.e. Fe, Mg, Mn, Ti) generate local imbalances on the crystal structure of tectosilicates and thus minerals like plagioclase do not host these types of elements in their crystal structure. Instead, large cations such as lead or Rare Earth Elements can be stored in the tectosilicate structures (Demange, 2012). The chemical compositions of common feldspars can be expressed in terms of the predominance of interstitial cations into three end-members: anorthite (Ca-rich), albite (Na-rich) and K-feldspars (Fig. 5a). There is complete solid solution (coupled substitution: $Na^+ Si^{4+} \Leftrightarrow Ca^{2+} Al^{3+}$) between albite (Ab) and anorthite (An) end-members, the group is called the plagioclase feldspars. The plagioclase composition is normally expressed in terms of its anorthite content (An_x). The feldspars whose compositions range between albite ($Ab_{10}Or_{90}$) and 100 % K-feldspars (Or_{100}) are termed alkali feldspars (Nesse, 1986). Solid solution on the alkali feldspars (K $\Leftrightarrow$ Na) exists only at high temperature (Stanley, 2017; Fig. 5b). At temperatures below 750°C two phases become stable (miscibility gap) in a single alkali feldspar grain, which are exhibited as exsolutions. The occurrence of different types of feldspar is associated with the temperature and composition. These effects have been addressed and schematized on phase diagrams presented and discussed by Laves (1952), Carpenter (1994) and Stanley (2017).

As most igneous minerals, feldspars become chemically unstable when exposed to Earth's surface conditions (Goldich, 1938). The rock-water interaction leads to the formation of weathering products through hydrolysis reactions. The feldspars ions (Na^+, K^+, Ca^{2+}) are released into solution to produce aluminum-silicate hydrated minerals (e.g. zeolites). In granitic rocks, alkali feldspars are more resistant to weathering by hydrolysis than plagioclase felspars. Also, the high-temperature Ca-rich plagioclase is preferentially weathered in comparison to low-temperature Na-rich plagioclase (Goldich, 1938). Zoned or cored plagioclases with an altered core and a fresh-looking rim are very common in igneous rocks and their preferential alteration is associated with the higher stability of sodic felspar versus lime-rich (Ca-rich) plagioclase (Goldsmith, 1952). In dry conditions, anorthite has very high melting point (~1550 °C) which is greatly reduced by increasing water pressure (Demange, 2012), the latter relationship between decreasing melting point with increasing water pressure holds true for most feldspars binary phase systems (Stanley, 2017) in igneous rocks, although the temperature stability in slowly cooled plutonic rocks is more similar to the schematic temperature ranges in shown in figure 5b.

The plagioclase solid solution allows the formation of chemical zoning, which commonly preserves the morphology of the crystal and the chemical variability of the medium during growth. The crystallization of feldspars from a mafic or intermediate melt generates normally zoned crystals with anorthite rich cores and albite rich rims, the opposite zonation is termed reverse zoning. Although there is solid solution between the alkali feldspars at high temperatures, at temperatures below ~700°C they tend to unmix into their end-members (Carpenter, 1994; MacKenzie et al., 1996). If there is enough time for crystallization the high-temperature alkali feldspars unmix into the low-temperature ordered varieties. The subsolidous unmixing process generates an intergrowth of fine-grained sodic (triclinic) and potassic (monoclinic) feldspars that can be observed at macroscopic and microscopic scales. This intergrowth is revealed by the presence of blebs or lamellae of sodic feldspar within potassium-rich feldspars (i.e. orthoclase or microcline). This texture is called perthite, and when sodic feldspar is the dominant phase it is termed antiperthite (Vernon, 2004). Unmixing solvi also occurs in on slowly cooling on plagioclase feldspars, but contrastingly to microscopic exsolution lamellae in alkaline feldspars, exsolution features of plagioclase cannot be observed with the optical microscope (Demange, 2012) and higher resolution techniques (i.e. X-ray Diffraction) are required for identification. In this study, the differentiation between plagioclase feldspars and alkali feldspars is primarily be based on the twinning and the optical properties visible under the petrographic microscope.
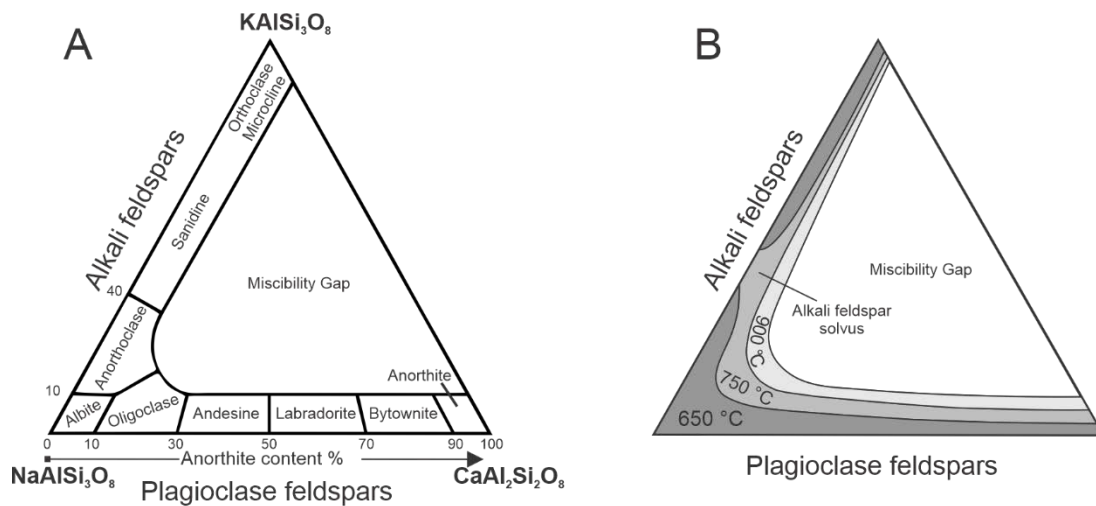
Figure 5. Felspar ternary diagrams. a) Composition of common feldspars modified from Neese (1986). b) Feldspar molar composition-temperature diagram illustrating the stability fields reproduced from Stanley (2017). The alkali exsolution solvus shown in b is the formation of two mineral phases, commonly known as perthite exsolution, from K-rich felspars during slow cooling at temperatures below 750 °C.

Quartz crystals form by precipitation out of silica-rich (> 50 wt.% SiO_2) melts. It is the second most common mineral in Earth's crust (Demange, 2012) and it the most stable of the six silica polymorphs. The other five silica polymorphs are only stable at very high temperature (i.e. crystobalite and tridymite) or very high pressure (i.e. coesite, stishovite) and commonly become into low temperature and low pressure α-quartz variety upon cooling. The low temperature and pressure stability of quart polymorphs (α and β) accounts for its great chemical and physical resistance to surface conditions (Goldich, 1938). The pressure versus temperature phase diagram presented by Demange (2012, pg. 53) clearly schematize the stability relationships between the silica polymorphs.

There is scarce research on hornblende megacrysts. Most of the geochemical, petrographic and petrologic studies related to megacrysts and/or pegmatitic textures are focused on K-feldspar megacrysts in either pegmatites or megacrystic porphyritic granites (Demange, 2012; Vernon, 2004).

2.2.3 *Classification of igneous rocks and granitoids*

Igneous rocks are the major constituents of both oceanic and continental crust. There is a wide variety of igneous rocks and their significance for understanding the evolution of orogens has been addressed in multiple works in literature (Barbarin 1990, 1999; Chew et al., 2007; Cochrane 2013, 2014a; Spikings et al., 2010, 2013, 2015). Most geologist use the systematics set up by the IUGS commission (Streckeisen, 1974, 1976; Le Maitre, 1989; Le Bas & Streckeisen, 1991; Le Maitre et al., 2005) to classify igneous rocks. The implementation of microscope petrography and geochemical analyses has increased the precision on the assessment of mineral phases and compositions. Thus, increasing the reproducibility of the results for rocks classified on standardized classification schemes.

These IUGS recommendations provide a comprehensive framework to classify igneous rocks based on their descriptive features, mostly related to texture, composition and mineralogy. The most common classification scheme used by igneous and metamorphic petrologist is the QAPF diagram first published by Strekeisen (1974). This diagram has been widely used to classify plutonic igneous rocks in terms of the modal amounts of quartz (Q), alkali feldspar (A), feldspathoid (F) and plagioclase feldspar (P). Modal percentages from thin section, hand samples or geochemical analyses can be plotted on a QAPF diagram (Strekeisen, 1991) but when geochemical information is available, the IUGS also suggests the use pf other discriminant plots (i.e. total alkali vs. silica), to schematize and compare the chemical signatures with the petrogenesis of the rock (see Le Maitre et al., 2005 for discussion).

In old zones of convergence, the volcanoes have been eroded to the point that only the remains of their granitoid batholiths (crystallized magmatic chamber) are exposed on the surface. One of the first attempts to classify granitoid rocks was made by Chappell (1974). He used mineralogy and geochemical signatures to tell apart different types of granitoids: I-type and S-type granites (Chappell, 1974). Further subdivisions on these two broad categories based on detailed geochemical models were later developed (Didier et al., 1982; King et al., 2001). The I-type granites are characterized by a) the occurrence of hornblende as the main mafic mineral, b) the high concentrations of sodium and calcium and c) chemical signatures of mantle affinity (Chappell, 1974). On the other hand, S-type are characterized by a) the occurrence of muscovite, biotite, widespread cordierite and > 1% of normative corundum, b) the sodium depletion and

aluminum enrichment and c) crustal isotopic signatures. I- and S-type granites are thought to form by partial melting of igneous and sedimentary rocks, respectively. The characteristics of these two types of granites are essentially related to its source material (Chappell, 1974; Chappell et al., 2001). There are several other classification schemes for granitoids published in literature and most of them share these common parameters.

Figure 6. A) Classification and nomenclature of igneous rocks according to their mineralogical contents using the QAP diagram; modified from (Streckeisen, 1976). B) Schematic table showing the relationships between the petrogenetic types of granitoids, their origin and the geodynamic environment; reproduced from (Barbarin, 1999).

The twenty most frequently used petrogenetic classification of granitoids were summarized by Barbarin (1990). The classification scheme of granitoids presented by Barbarin (1990) link the petrography, mineralogy, and chemical characteristics of granitoids with their origin and tectonic setting. His scheme based on a comparison between the twenty most frequently used petrogenetic classifications for granitoids uses descriptive parameters such as nature and abundance of enclaves, major and trace element, isotope geochemistry, radiometric dates and mineralogy of granitoids as indicators of their origin and geodynamic environments. His classification was further refined by himself (Barbarin, 1999) in which he emphasizes that the combination of petrologic, structural and geodynamical data pinpoints that the genesis of different types of granitoids is strongly associated with the prevailing geodynamic environment. Calc-alkaline igneous rocks are associated with subduction-related magmatism (Barbarin, 1999). This type of igneous rock form by the fractional crystallization of magma following the calc-alkaline fractionation trend. The calc-alkaline trend shows very little iron enrichment due to continuous crystallization of magnetite (Fig. 4a).

3. *Materials and methodology*

The methodology employed for the development of this study involves the compilation of appropriate literature, sample collection and processing and the redaction of the written document. A 12-m resolution Digital Elevation Model (DEM) from ALOS PALSAR was used for the construction of the maps. The maps presented have WGS1984 datum and are projected on the UTM 17N coordinate system (Figs. 2, 7). They were made with the aid of ArcMap 10.2 and Corel Draw 2019. Field description and sample collection were performed on road cuts. Petrographic description of hand samples was performed and used to select samples for the thin section preparation. Rock chips were made and sent for thin section's preparation at Wagner petrographic laboratories, USA. The thin section petrography was performed with the aid of an Olympus BX-150 Polarized Light Microscope available at Yachay Tech.

3.1 Thin section petrography

The identification of minerals in thin section is based on the protocols for thin section petrography described by Raith et al. (2011) and the properties described by Nesse et al. (1991). While the aim of this study is not to teach how to recognize minerals in thin sections, some of the parameters used overall to describe the size, composition and textures of mineral grains under thin section are presented in Vernon (2004) and were briefly described in the Chapter 2.2. The interpretations of the mineral paragenesis and rock microstructure were mainly based on Demange (2012) and Vernon (2004) but experimental results from analogous studies are also considered.

The determination of modal percentages was made through the Point Counting Method (PCM) under the Olympus Polarized Light Microscope. A 20x20 points grid with 0.1mm spacing was over imposed on the digital views of the thin section under the microscope and were used as reference for the point counting of ~400 points in four areas of the two thin sections of the Pimampiro pluton (MOL-01A, MOL-01C).

The systematic variation in the extinction angle of plagioclase twins was measured under Cross Polarized Light (XPL) on the petrographic microscope and was used to determine the plagioclase composition. The Michel-Levy method was used to determine the albite and anorthite components of plagioclase in thin section. This method for determining plagioclase composition is based on the extinction angle of albite twin sets in appropriately oriented mineral grains. The procedure used for the selection of plagioclase grains, the measurement of their extinction angles and the conversion to compositions is the one described by Nesse (1991).

3.2 Igneous rocks classification scheme

The classification schemes of Streckeisen (1974) and Barbarin (1999) were used in this work because of their applicability with the type of data presented in this study to precisely classify the rocks from the Pimampiro pluton and to relate them to a geodynamic environment. The classification of igneous rocks in this thesis work follows the International Union of Geological Sciences (IUGS) recommendations namely IUGS Systematics of Igneous Rocks Classification (Le Bas & Streckeisen, 1991). The QAP diagram commonly employed for the classification of igneous rocks is used when the amount of mafic minerals is less than 90%. The modal percentages of quartz

(Q), alkali feldspar (A) and plagioclase (P) obtained with the PCM on thin sections were normalized to 100% in order to plot these values in the ternary classification of Streckeisen (1974).

In the case that mafic plutonic rocks exhibit marked effects of dynamic metamorphism, appropriate metamorphic names will be used instead of the plutonic names. Textural terms are used as prefixes of the rock's name so that the effects of dynamic metamorphism, if any, are clearly and properly indicated. Name modifiers are used for igneous rocks in companion of the regular name. It is important to notice that the names provided to volcanic rocks are provisional since quantitative geochemical analyses are required before assigning a proper name in the scheme of the IUGS normative mineralogy classification system (Le Maitre, 1989). The petrogenetic classification of Barbarin (1999) assigned in this work is based on the mineral association of the rocks elucidated through the detailed petrographic description. Although the geochemical data from the pluton is not available to further confirm its classification, the mineral paragenesis is consistent enough that a clear distinction can be made between the proposed category for the Pimampiro pluton and the other categories in the scheme of Barbarin (1999).

4. *Descriptions and results*

Field and petrographic observations are described in this chapter in terms of lithological units. Thin sections of the characteristic lithologies are presented and detailed descriptions are included. These descriptions are used to identify the mineralogy, rock type, lithological unit, and the corresponding terrane. The name of the lithologies and terranes of the Cordillera Real defined by Aspden and Litherland (1992) are employed when possible (Fig. 7).

4.1 Pimampiro pluton: MOL-01A, MOL-01C

From west to east, following the road from Ambuquí to Monte Olivo or from Pimampiro to Chuga, the first outcropping igneous lithology is the Pimampiro pluton (Fig. 7). It stands out as a high relief steep-sided mountain that reaches a height of 3121 masl (Fig. 8a). The rocks are ubiquitously fractured and weathered (Fig. 8b). The Pimampiro pluton is considered the oldest of the "virtually non-deformed" post-metamorphic plutons of the Cordillera Real according to Litherland et al. (1992) as most of older pluton show metamorphic characteristics.
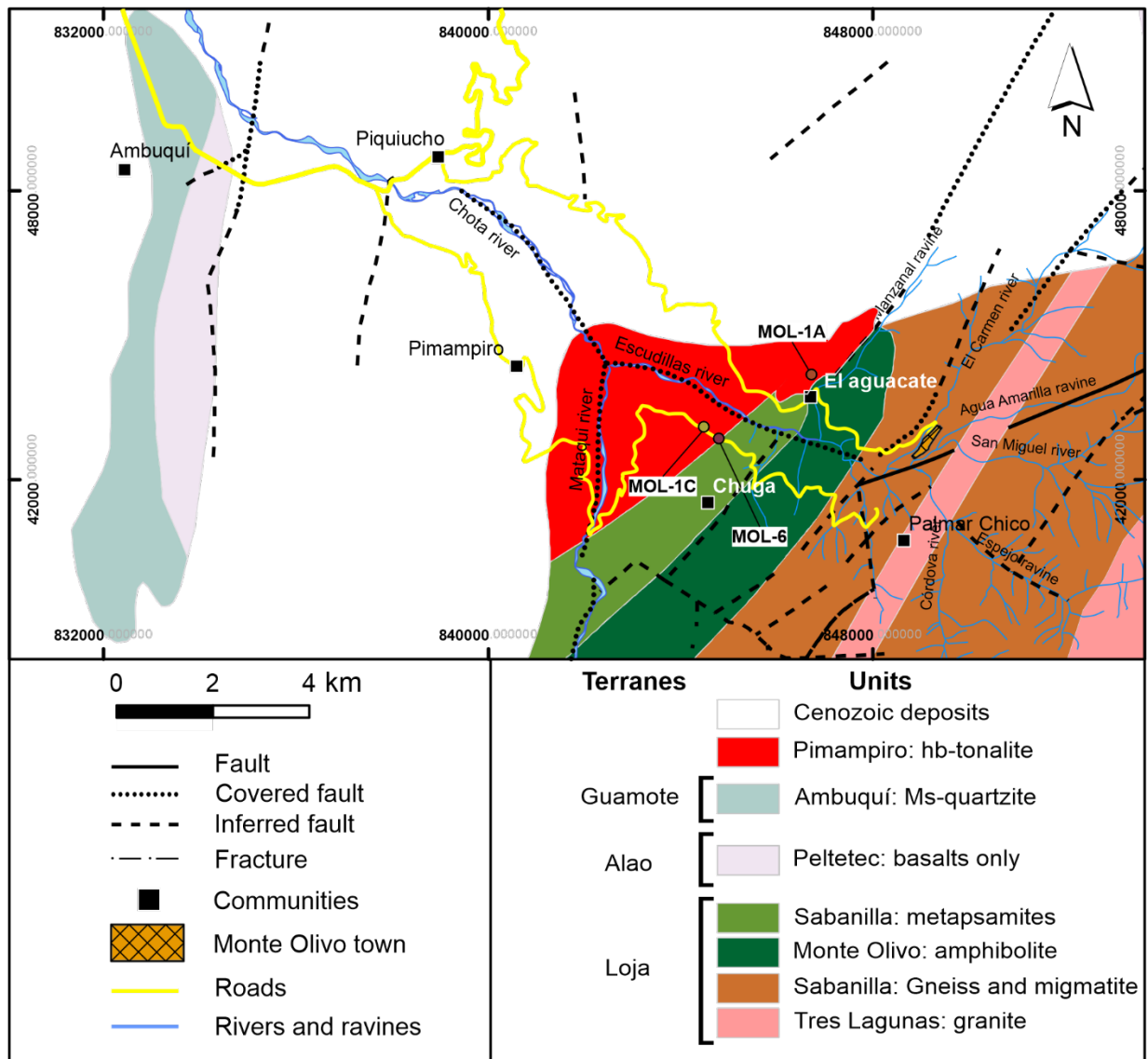
Figure 7. Geological map of the study area showing the Pimampiro hornblende (hb) tonalite and the metamorphic units of the Guamote, Alao and Loja terranes described in this study. The Ambuquí and Monte Olivo areas, and locality of selected thin section samples described are shown. Geologic cartography was modified after San Gabriel geologic sheet (Salazar et al., 1986) and Litherland et al. (1994).
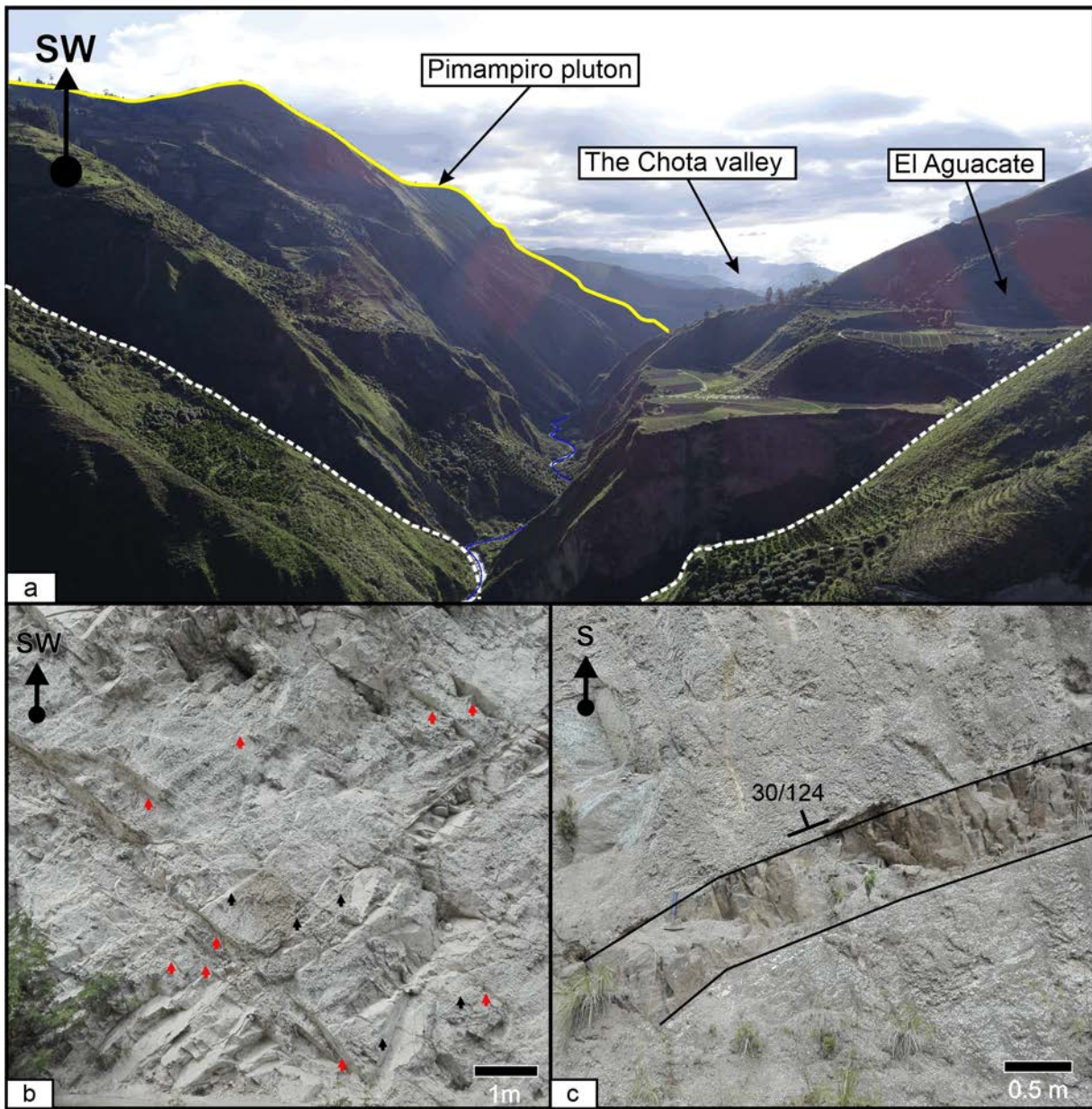
Figure 8. Panoramic image of the Pimampiro pluton along the Escudillas river valley (a) and characteristic outcrops (b-c). a) Panoramic view of the Pimampiro pluton (yellow line) and its eastern contact (white dashed) inferred to be along the Manzanal ravine, east of the El Aguacate town where there is a marked lithological and metamorphic change. The Chota valley, further west, receives the sediments from the Escudillas river (blue line). b) Outcrop scale fracturing of the pluton. Pervasive crosscutting sets of fractures (red and black arrows) are affecting the pluton and facilitating weathering. c) Isolated mafic dike cutting the pluton with dip and dip direction (30/124). The view direction is shown in the upper left corner of each image.

29
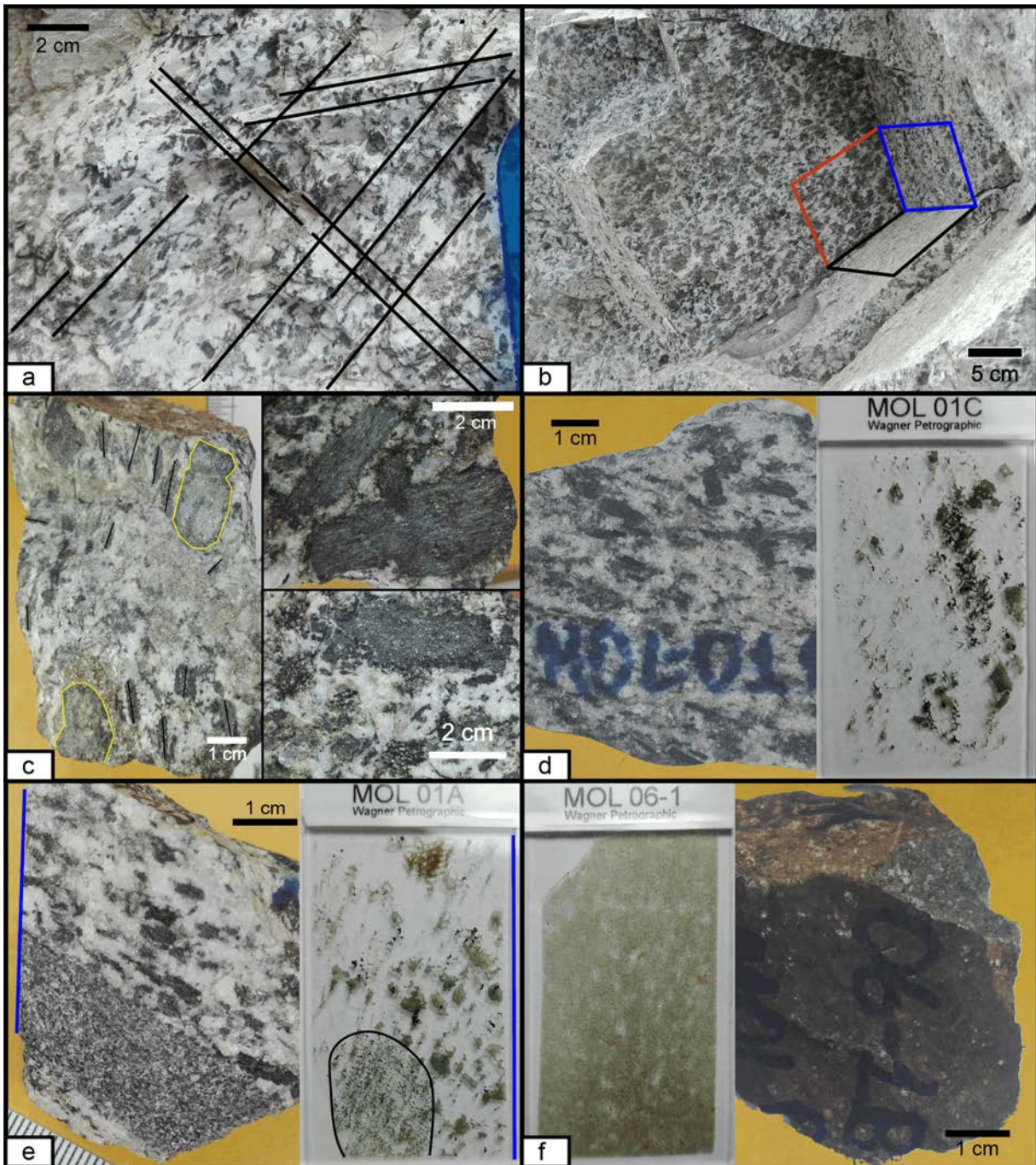
Figure 9. Field and hand sample photographs of the Pimampiro pluton hb-tonalite (a-e) and basaltic intrusion (f) shown in figure 4c. a-b) Outcrop images with amphibole (a) and biotite (b) megacryst and phenocrysts, and fracture sets (red, blue and black planes); notice megacrystic biotite on the red plane. c) Amphibole megacryst with marked zonation (yellow upper center and lower left) and parasitic twins (upper and lower right). Thin section photographies of corresponding hand samples (d-f) are approximately 4.5x3 cm (length & width). Blue solid lines (e) indicate the sectioning plane of MOL-01A (4.5 cm long) and the black segments outline a mafic microgranular enclave (MME) in the host hb-tonalite.

The Pimampiro pluton is an intermediate intrusive rock with a megaporphyritic texture given by around 35% mafic minerals (amphiboles, dark micas) and 65% phaneritic matrix composed by a felsic assemblage (plagioclase and quartz). In hand sample, mineral grain size of the Pimampiro pluton ranges from ~ 2mm to ~4 cm. The pluton is composed of seriate amphiboles (megacrysts and phenocryst to fine grains), and phenocrystic plagioclase and quartz (Fig. 9a-e). The Pimampiro pluton variably displays tonalite rocks with abundant amphibole megacrysts (pegmatitic) and occasionally megacrystic biotite (Fig. 9b). The very coarse amphibole megacrysts (> 3 cm) are mostly actinolite cores rimmed by hornblende. Parasitic fine-grained twins are very common on the crystal faces of the larger grains (cyan lines on amphiboles). In thin section the felsic mineralogy of the Pimampiro pluton is mainly dominated by plagioclase and minor quartz and muscovite while the mafic phases are mainly actinolite, hornblende and biotite with minor chlorite and epidote (Fig. 10a-b, e-f). Accessory apatite, opaques (mostly magnetite), and clays are also present in small traces. The mineralogy of the microgranular enclave (ME) outlined in thin section MOL-01A is identical to its host mineralogy (Fig. 10c-d).

The amphiboles (calcic clinoamphiboles) present in the Pimampiro pluton show a bimodal distribution in both hand sample and thin section. There are megacrysts (>30 mm) of ferro-actinolite to actinolite affinity (Fig. 9c) and phenocrystic hornblende (Fig. 9a-e). The shape of the megacrysts varies with their size. The large amphibole megacrysts are mostly euhedral and their surface are sometimes rough with parasitic smaller amphiboles on its crystals faces. Subhedral amphibole grains (~ 1cm across) constitute the most abundant mineral size in the pluton. In thin section, the bimodal distribution of amphiboles is marked by the occurrence of phenocrysts and microcrystalline clinoamphiboles with absent zoning (Fig. 11) and phenocrysts with marked patchy zoning (Fig. 12). In general, the amphiboles have a strong pleochroism that varies from yellow to green to pale blue (Figs. 10, 12). The grains whose X axis are parallel to the lower polarizer direction (E-W) show pale yellow-green colors while those with its Y axis aligned display dark green and those with its Z axis aligned in the E-W direction show green-blue to light blue. Interference colors range from second order yellow to purple and are sometimes masked by the true mineral color. Under PPL the amphiboles show medium to high relief compared to plagioclase and quartz. The characteristic cleavage planes of amphiboles {110} intersecting at angles of 56° and 124° (Nesse, 1991) are visible under both PPL and XPL at grains cut in sections close to or perpendicular to their c-axis (Fig. 11e). Most of the phenocrystic amphiboles exhibit simple twinning (Fig. 11). In some cases, the simple twins are pseudomorphed by epidote of the pistachite type characterized by its pistachio interference colors (Figs. 11d, 12b). Subhedral plagioclase indenting large amphiboles (Figs. 10a, 11c) is a common characteristic observed on thin section. Extinction is inclined on elongate amphibole grains and symmetrical on basal (equant) sections. The

amphiboles megacrysts show marked patchy color-zoning (Fig. 12a-d) and the outer rims of these larger grains show smaller extinction angles than the cores (Fig. 12a-b).

Although it may seem that there is mineral lineation of the Pimampiro pluton amphiboles, amphiboles and plagioclase observed at both hand samples and thin section samples do not exhibit strong alignment rather show granular texture. The groundmass of the Pimampiro pluton is formed by anhedral to euhedral plagioclase (up to 1 cm long) and interstitial quartz grains. Under plain polarized light (PPL) plagioclase feldspar display a variety of disequilibrium textures (Fig. 13). They are transparent subhedral low-relief grains. Traces of twinning (green, purple, yellow lines) and zoning planes (blue lines) discernible in some grains under PPL become ubiquitous under cross-polarized light (XPL). Plagioclase grains featuring polysynthetic albite twinning (green), pericline twinning (purple) or a combination of these are present (Figs. 10, 13). Sericite alteration (clay) of plagioclase grains is very common in the Pimampiro pluton. Alteration to very fine clays gives a cloudy (brownish) texture to plagioclase grains under PPL (Fig. 10a, e). Under XPL, the altered zones show third order interference colors (Fig, 10b, f). The sericite alteration is well developed at the cores of zoned plagioclase crystals (red polygons) and along alternating bands of zoning (Fig. 10e-f). Oblique extinction (~21°-24°) and zoning are common in the large plagioclase crystals (>5 mm). The composition of plagioclase feldspar was obtained through careful measurement of extinction angles of several appropriate grains. According to the Michel-Levy method, the average anorthite component of plagioclase feldspar in the Pimampiro pluton range from An38 to A45. This composition falls into the Andesine group of plagioclase feldspars as schematized in figure 17.

Quartz is presents as low-relief anhedral grains in the Pimampiro pluton. Commonly transparent with marked inclusion trails, fracture sets and ubiquitous ondulatory extinction in the quartz grains serve as distinctive features to differentiate them from plagioclase. Most of the grains show irregular lobate boundaries (Fig. 10b, f) and/or serrate borders (Fig. 14). The contact between quartz grains is serrate-undulose, while the plagioclase-quartz grain boundaries are straight to undulose. In contrast to the previous, the contacts between amphibole and biotite are straight with well-developed biotite crystalline faces (Fig. 11a, 12c). Epidote is present in small traces associated with amphiboles, biotite and chlorite. Epidote shows a slight pleochroism from light to dark yellow with second order orange maximum interference color. It has a medium to high relief compared with plagioclase and features no cleavage. The grains are completely stained of fine-grained opaque inclusions. Pistachite-epidote is the most common variety present. It is characterized by its pistachio interference color. Most grains are pseudomorphing amphiboles either completely or half twins (Figs. 11c-d, 12b).
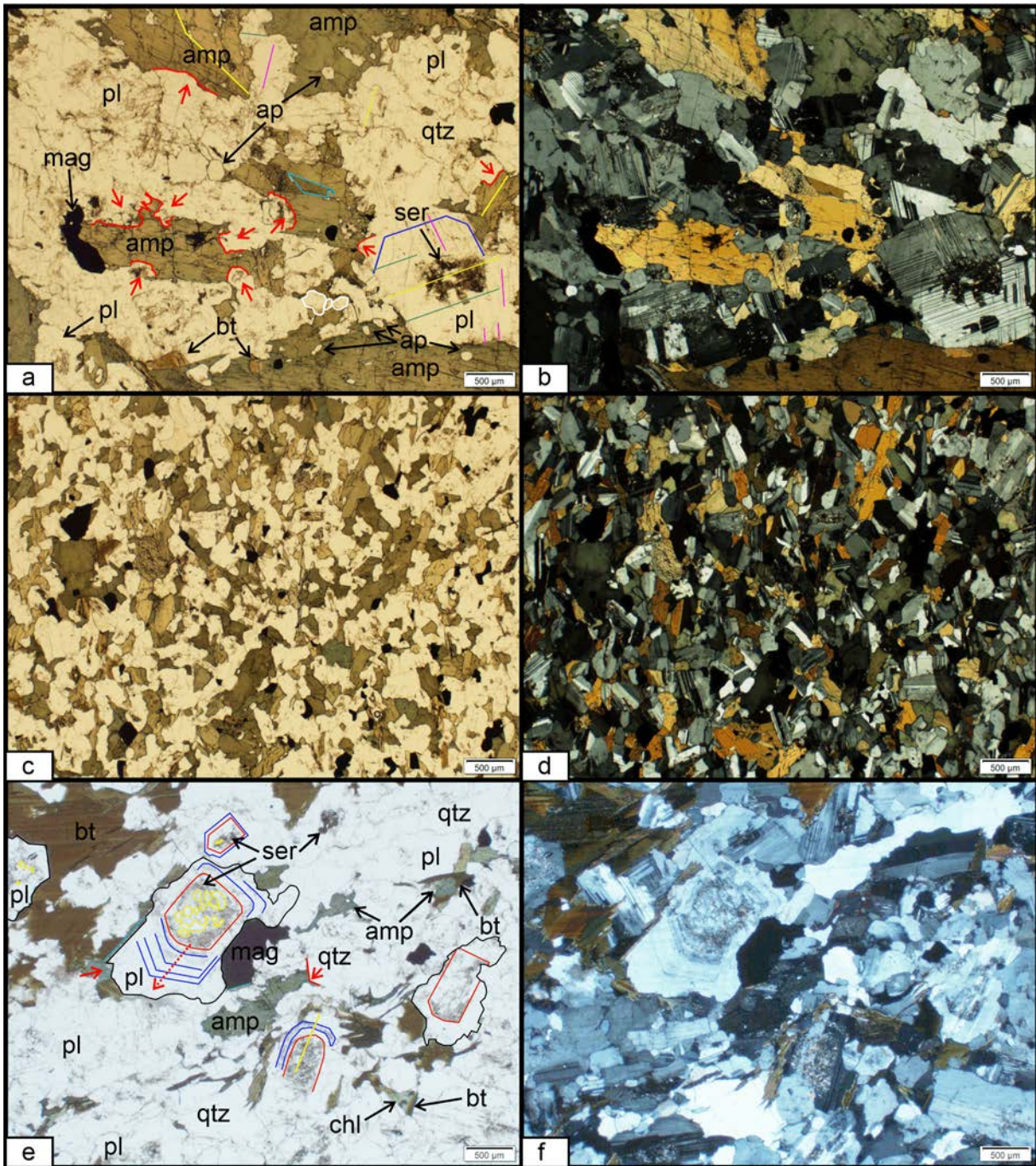
Figure 10. Microphotographs of thin sections MOL-01A and -01C with characteristic mineralogy and disequilibrium textures. a-b) Inclusion rich amphibole phenocrysts indented (red lines and arrow) by anhedral plagioclase with sericitized cores. Quartz grain on the upper right has a melting texture. c-d) Microgranular texture of enclave shown in Fig. 11e. with identical mineral assemblage to a-b. e-f) Zoned plagioclase crystals and large "book" of brown biotite. Scale of each picture is shown on the lower right corner. XPL images are shown on the right and PPL are shown on the left.
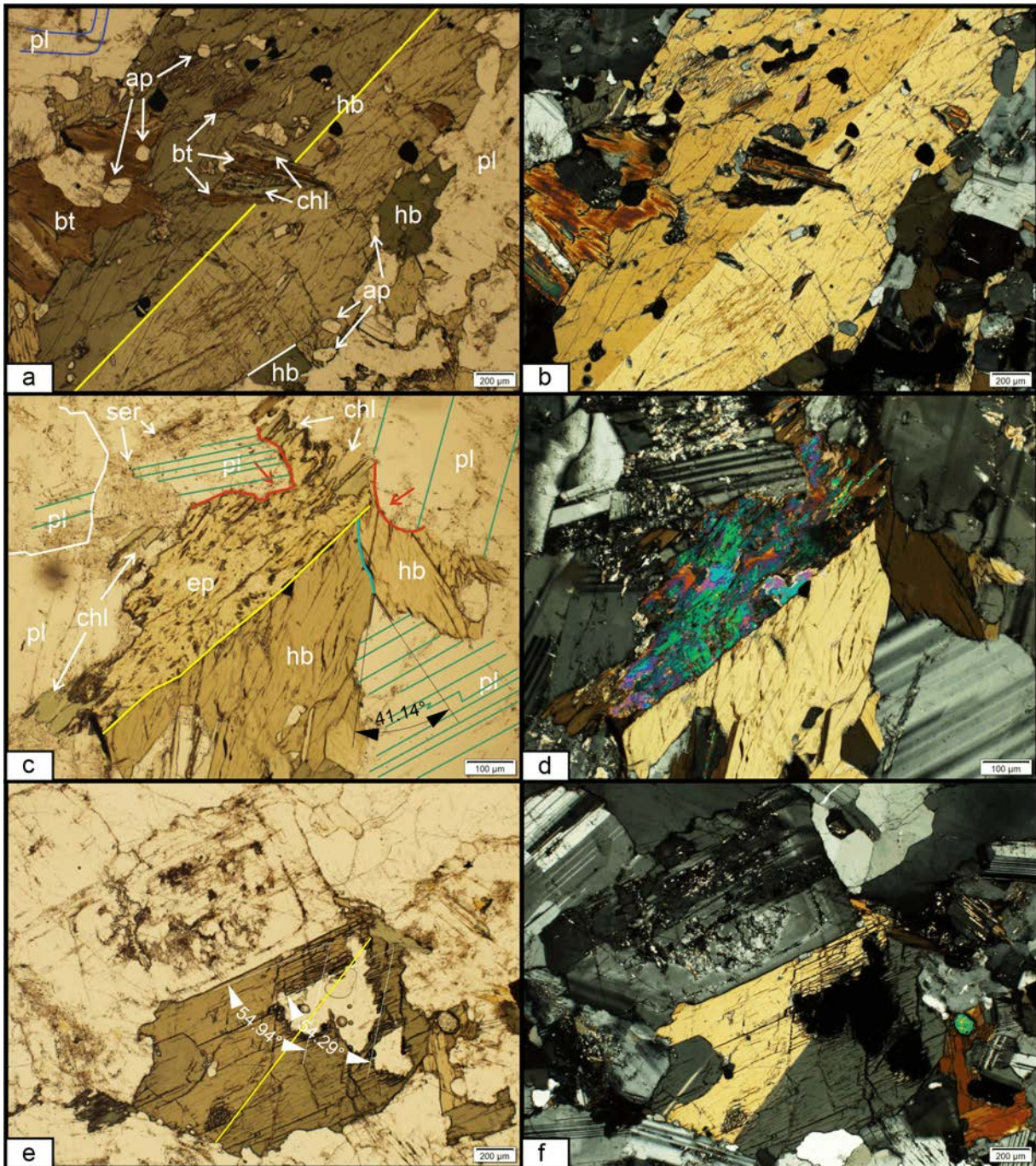
Figure 11. High magnification (10x and 40x objective) microphotographs of calcic amphibole phenocrysts in the Pimampiro pluton. a-b) Twinned amphibole rich in apatite (hexagonal and prismatic sections) inclusions. Chloritization of biotite is marked by color and relief change under PPL. c-d) Epidote (pistachite) pseudomorphing an amphibole simple twin. e-f) Penetration twin between amphibole and zoned plagioclase with sericitized cores. The upper left border of the large plagioclase shows dissolution textures. Scale varies between 100 and 200 µm.
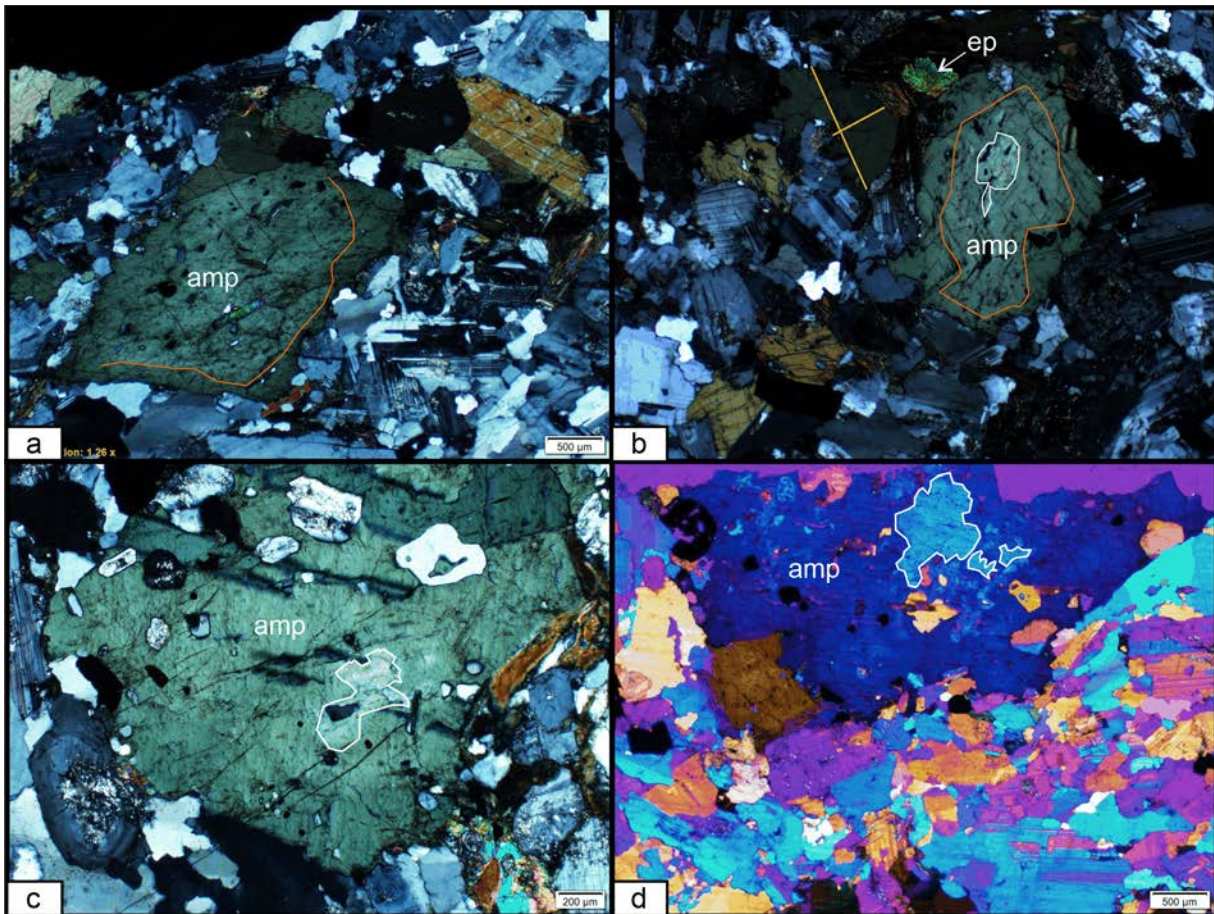
Figure 12. Microphotographs of calcic clinoamphiboles megacrysts with irregular color zoning under XPL (a-c) and with the gypsum plate inserted (d). a) Large pale-green core of amphibole full of inclusions and a darker rim with slightly smaller extinction angle than the core. b) Small pale green irregular core (white polygon) in large amphibole. Notice the transition from the light-green core to the dark-green rim and the presence of pistachite on the upper center. c-d) Amphiboles with irregular pale-green patchy-zoned cores (white) and darker rims. White lines show patchy zoning and orange line separate darker rims from lighter cores. Yellow intersecting lines show the hour-glass zoning planes on an amphibole at near extinction position.

Euhedral apatite crystals are present as ~50-100 µm inclusions inside amphibole grains (Figs. 10a, 7a). The larger crystals are bounded by the felsic assemblage. Inclusions of apatite inside mafic minerals are considerable smaller (~50 µm) than the crystals associated with the felsic mineralogy (~200 µm). The apatite crystals are invariably transparent under PPL and show up to first order bluish grey interference color under XPL. Most sections shown in the thin section are hexagonal (basal sections) and have a medium to high relief compared with amphiboles and plagioclase respectively. Elongate prismatic sections are also shown (Fig. 10a)
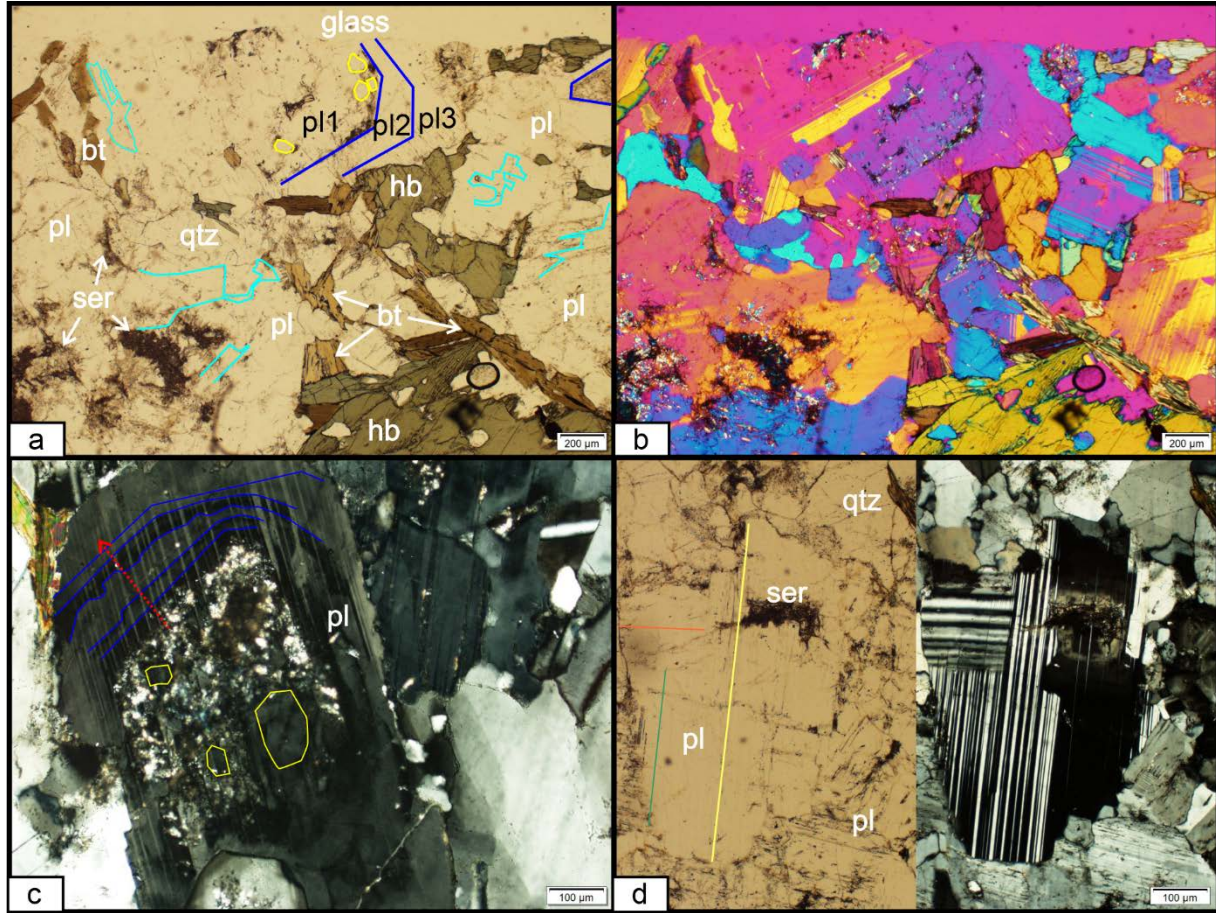
Figure 13. Disequilibrium textures on plagioclase. a-b) Zoned plagioclase with sericitized anhedral core (blue). Patchy zoning on the altered core is reflected by unaltered relict plagioclase (yellow). Skeletal growth (cyan) is visible with the gypsum plate inserted (b). c) Oscillatory zoned rims (blue) and patchy zoned core (yellow) on plagioclase. Note the reabsorbed (not straight) oscillatory zoning. d) Corroded border of plagioclase (upper left) with characteristic albite twinning (green) and a penetration twin (yellow).

The mineralogy of the sample MOL-01C is more or less the same than sample MOL-01A therefore, only distinctive characteristics will be described for the sample MOL-01C. Most of the plagioclase from this sample show concentric oscillatory-zoned euhedral cores mantled by anhedral rims in optical continuity with its zoned core (Figs. 10e-f, 11c-d). Few deformation twins are present compared to growth twins (albite, pericline), which are pervasive across the whole sample and in most cases partially overwrites previous textures (zoning). The inner cores of zoned plagioclase grains are ubiquitously altered to sericite, which in some cases pseudomorphs the core crystalline faces. This alteration is not restricted to the cores but also to the low-birefringence

(darkest) bands on medium grained zoned plagioclase (Fig. 10e-f). Alteration of plagioclase to sericite (talc) is also present lengthwise to the twinning planes of cored-grains. The outer euhedral rims of most cored plagioclase are little altered (sericite) to unaltered. The anhedral rims are delineated by numerous very fine-grained inclusions. These zones are commonly surrounded and indented by anhedral to subhedral biotite (Fig. 10e-f).
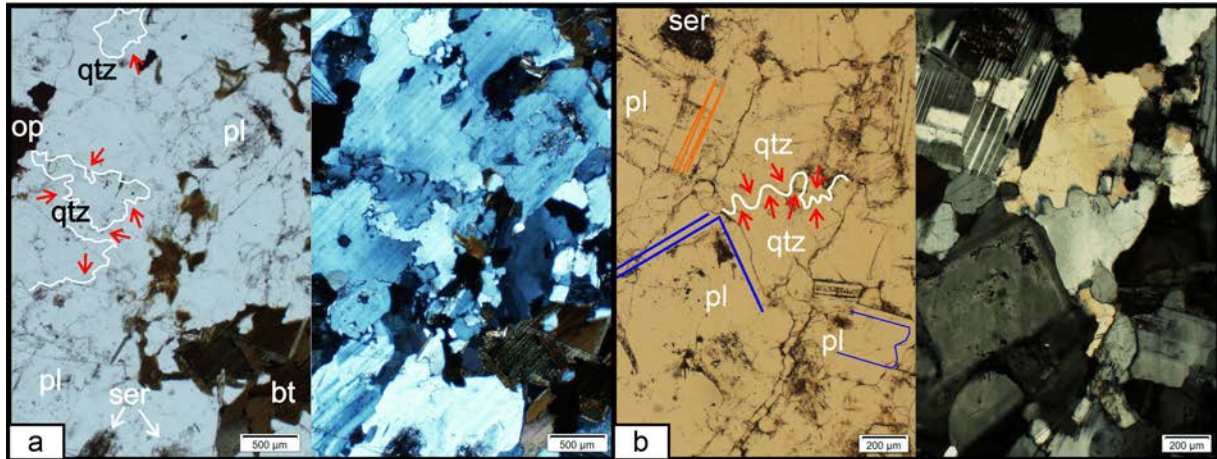
Figure 14. Recrystallized quartz grains on PPL (left) and XPL (right). a) Serrate boundaries (white line) produced by recrystallization of a single quartz grain into multiple subgrains. b) Zoned and twinned plagioclase, and recrystallized quartz grains. Undulose limit (while lines) at quartz-quartz subgrain boundary. Orange spikes delineate growth twins on plagioclase against a quartz grain.

Biotite is moderately pleochroic from light to dark brown in thin section. Cleaved and non-cleaved planes are shown in this sample. Cleaved faces show the typical bird's eye extinction under XPL and display fourth order green as maximum interference color. The interference color of non-cleaved faces is masked by its dark brown color. Biotite is partially replaced by chlorite. Inclusions of biotite on large amphibole show a higher degree of alteration to chlorite (Figs. 10a-b, e-f, 11a-b).

Quartz inclusions are present in some biotite grains. The quartz inclusions have regular sweep undulatory extinction. Non-inclusion quartz grains show features of melting and grain boundary recrystallization (Fig. 11g-h). Apatite is also present as tiny inclusions in both the matrix and in most amphibole grains. There are also subhedral amphibole inclusions whose long axis are parallel to the host plagioclase lamellar-twin planes. Large amphibole phenocrysts are overgrown by euhedral zoned plagioclase. The subhedral amphibole grains show undulose boundaries with euhedral plagioclase.

4.1.2 Mafic microgranular enclaves

The mafic and intermediate enclaves of the pluton have a much finer equigranular texture and a darker color than the host rock (Fig. 15). Mafic microgranular enclaves have the same components as the host tonalite; only the proportions and size of minerals are different. Texturally, the enclaves range from being microgranular to porphyritic but in general, plagioclase and amphibole are much finer than in the host rock.

The edges of the microgranular mafic enclaves are well defined (Fig. 15a,b,d) and their distribution is irregular and not restricted to any specific part of the pluton. The contacts with the host tonalite are sharp and chilled margins have not been observed. Although in some areas there is a greater concentration of enclaves than in others, due to the scarcity of outcrops it cannot be clearly established if these form swarms. The enclaves have elliptical and blocky shapes with sharp boundaries. They vary in size between 5 and 60 cm long although the great majority does not exceed 10 cm in diameter. In the central parts of the pluton the enclaves have more ellipsoidal shapes, like drops and biotite is the dominant mineralogy in these enclaves in comparison to the hornblende-rich compositions of most enclaves sampled.

The contrast in shape between the blocky enclaves on the outer borders of the Pimampiro pluton and the drop-shaped ellipsoidal enclaves in the central parts of the pluton can be associated with the differences in viscosity of the mafic and felsic magma. At the borders of the pluton, the temperature is closer to the solidus than the inner parts, therefore the contrasting difference in temperature and viscosities between the felsic host and intruding mafic magma allows the transport of mafic batches as rigid bodies (Vernon, 2004). The mafic magma is more undercooled relative to the host with respect to the liquidus temperature, this induces rapid crystallization of minerals in the mafic magma and produces the microcrystalline texture on the enclaves.
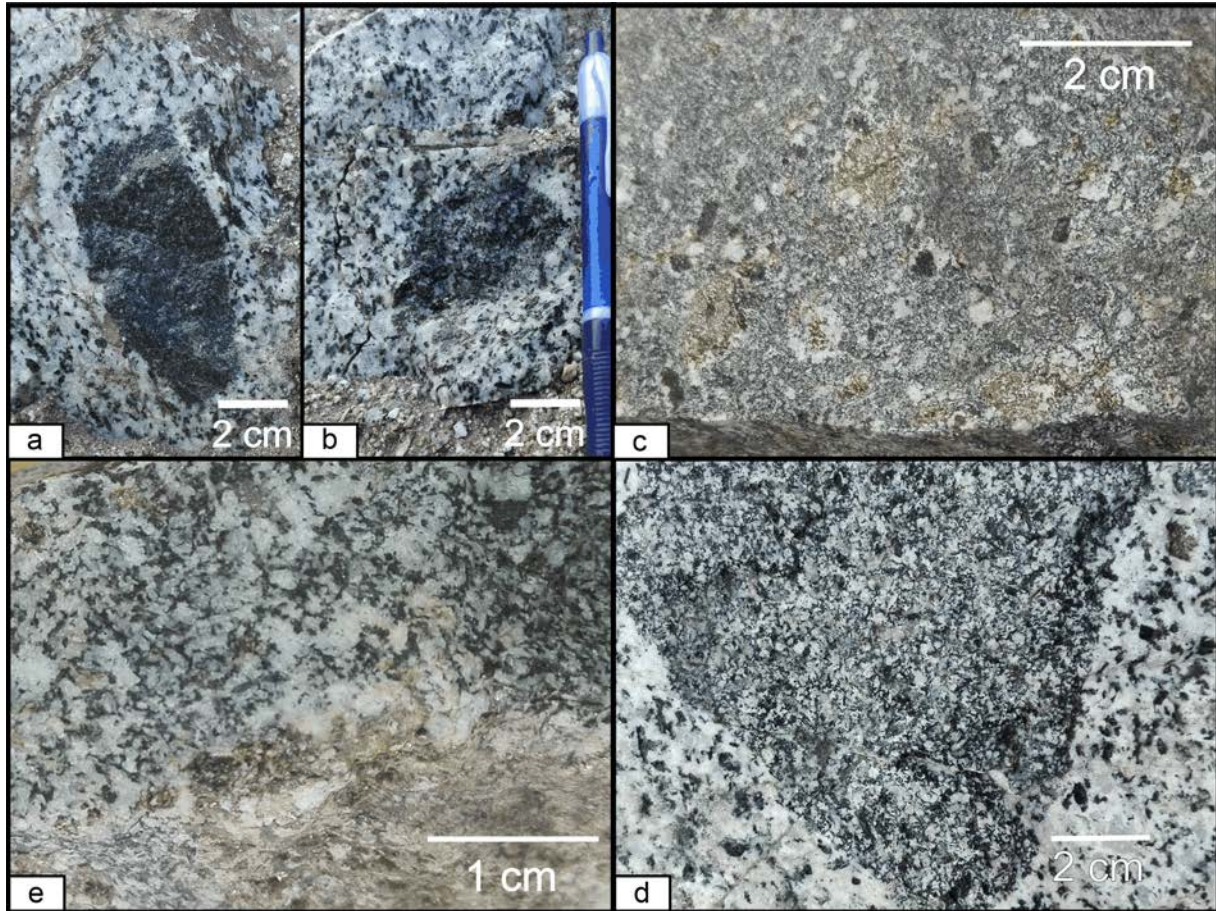
Figure 15. Representative mafic microgranular enclaves in the Pimampiro pluton (a-e). Notice the variability of the color index and coarseness. The finer grained enclaves (a-b) are the product of greater thermal disequilibrium with the host felsic rock. The sharp boundaries are preserved when viscosity contrasts are high enough such that the mafic melt is transported as a rigid body.

4.1.3 Mafic intrusion on the Pimampiro pluton: MOL-06

The basaltic dike found during our exploratory campaigns is heavily altered and weathered, as well as its host hornblende-tonalite (Fig. 8c). The basalt hand specimens are melanocratic, holocrystalline, medium-grained and porphyritic. The main mineral phases pyroxene, plagioclase, prehnite and opaque minerals (mainly magnetite). The secondary minerals include uralite, sericite and chlorite. In thin section, the mafic dike has a cummulophyric texture made of orthopyroxene and feldspar clusters embedded in a finer matrix of feldspar laths, pyroxene, opaques and chlorite (Fig. 12a-d). Other textures visible

under the microscope are intergranular, glomerophyritic and amygdaloidal textures. There are euhedral to subhedral crystal fragments of orthopyroxene (opx) with interference colors up to 1st order orange and red, some of which show irregular zoning. The dike is stained by fine-grained opaques (Fig. 16e-f). Wide depletion haloes around subhedral to euhedral phenocrystic plagioclase are present (Fig. 17a-b). The plagioclase phenocrysts are almost completely replaced by prehnite (Fig. 17c-d) and minor epidote at the cores. The mafic mineralogy is replaced by low relief fine-grained chlorite, uralite and serpentinite (Fig. 17e-f). The feldspar laths in the matrix are highly altered into fine grained mica.

Alteration to epidote at the expense of plagioclase is a retrograde metamorphic reaction. At medium metamorphic grade conditions Ca-rich (anorthite) component of the plagioclase provides the calcium for the formation of epidote (Vernon, 2014) and Ca-poor plagioclase (albite) through the following reaction: An = Ep + Ab (Fig. 17 c-d). The albite was later pseudo-morphed by prehnite at a lower metamorphic grade. Uralitization of mafic minerals (i.e. pyroxene) is associated with alteration phases such as chlorite and serpentinite (Vernon, 2004).

The occurrence of this mafic tabular intrusion on the Pimampiro pluton can be associated with the fourth type of interaction between felsic and mafic magmas described by Barbarin & Didier (1992) in which the intermediate host rock (Pimampiro pluton) has already crystallized enough so that the temperature and viscosities of the new mafic intrusions cut the felsic pluton as a rigid body. The temperature and viscosity conditions of mafic magma injecting at this point (Fig. 8c) should lie outside the windows of mutual deformability, meaning that the mafic magma or enclaves are transported as rigid objects in the host felsic magma (Caricchi et al., 2012).
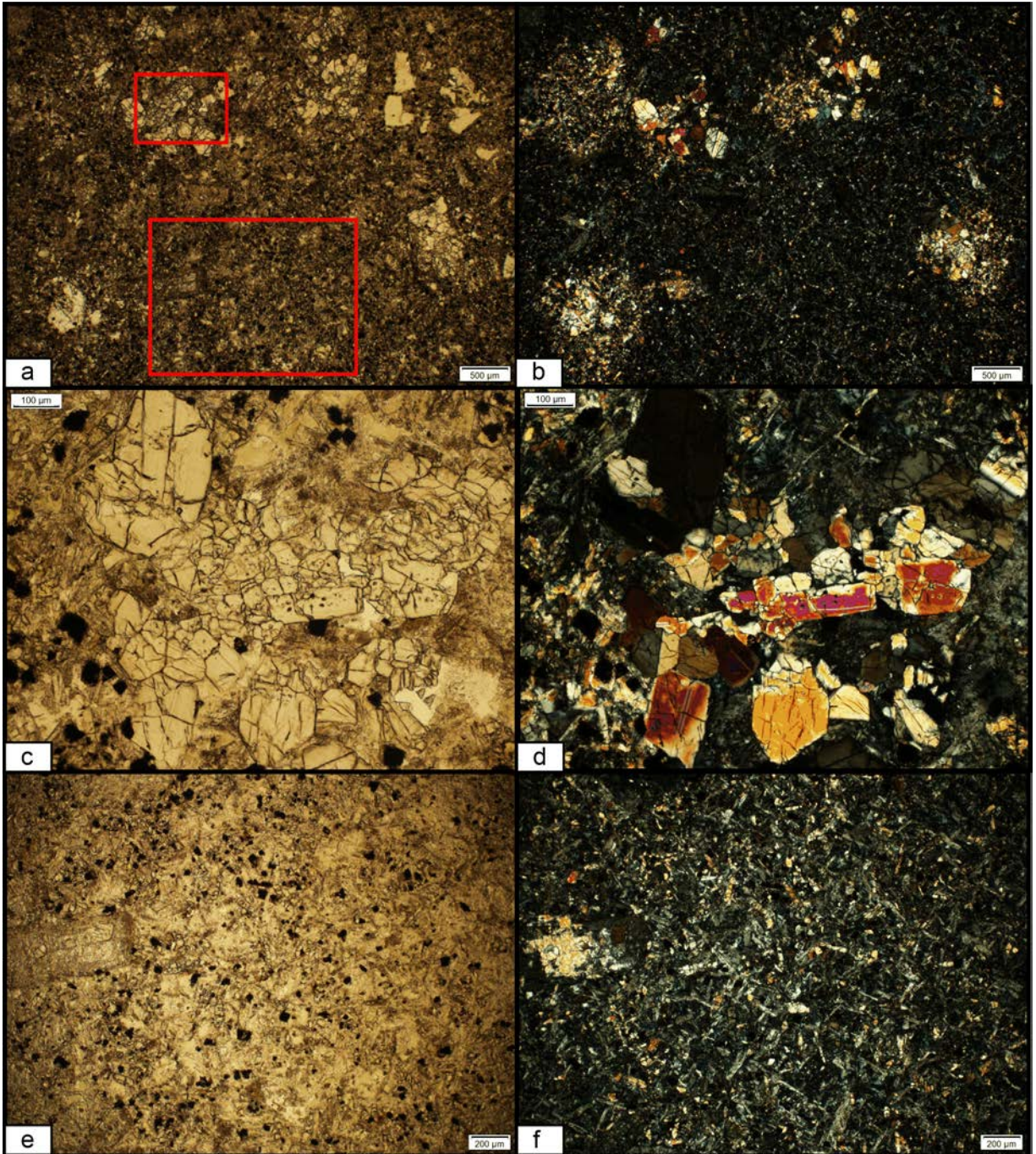
Figure 16. Microphotographs of sample MOL-06A, a mafic dike cutting the Pimampiro pluton: PPL on the left column and XPL on the right column. a-b) Texture of the mafic dike and mineral assemblage. Small and big red rectangles shown the location of c-d and e-f detail images, respectively. c-d) Glomerophyritic orthopyroxene. Notice the irregular zoning reflected by changes in the interference color of core and rims of single pyroxene grains.
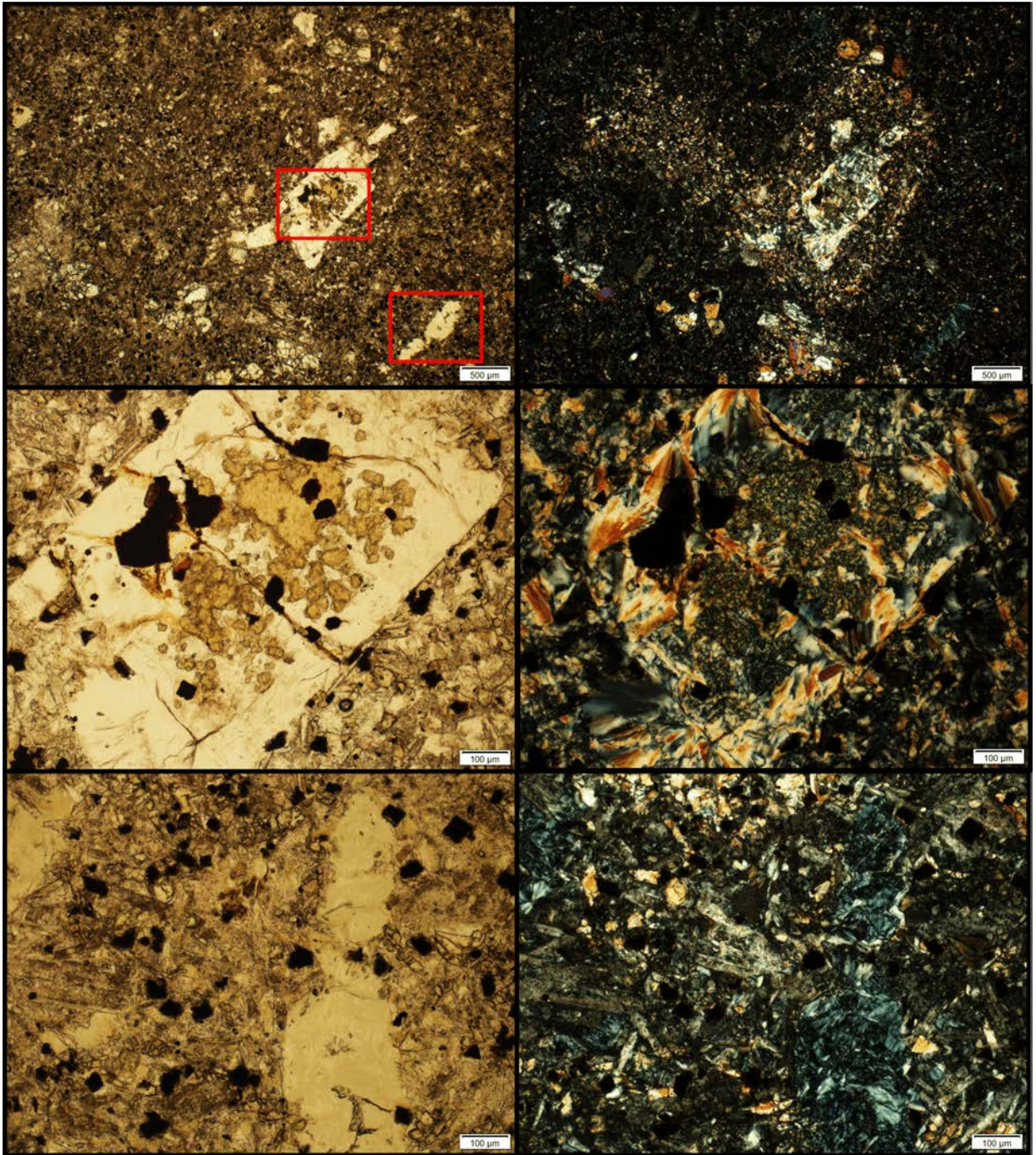
Figure 17. Microphotographs of typical alteration of major phases in sample MOL-06A; PPL on the left column and XPL on the right column. a-b) Depletion halo around plagioclase phenocryst that becomes evident under XPL. Red rectangles show location of detail images (c-f). c-d) Prehnite after subhedral plagioclase. The inner core is altered to epidote. Notice overprinting of opaque magnetite, which are widespread on the dike. e-f) Chlorite after mafic phases (Px). Notice the widespread subhedral plagioclase lath composing the matrix and pervasive magnetite.

4.2 Petrogenetic classification of the Pimampiro pluton

The extinction angles of 25 measured grains of plagioclase in the Pimampiro pluton range from 21° to 24°. According to the curves of Tobi and Kroll (1975), this extinction angles correspond to compositions between An_{38} and An_{45}. This compositional range of plagioclase feldspar grains in the Pimampiro pluton measured with the Michel-Lévy Method is shown as a red bar in figure 18. These compositions represent an average bulk Andesine composition for the measured grains. The modal percentage of plagioclase, quartz and alkali feldspars (absent in thin section) assessed through the Point Counting Method (PCM) are presented in the QAPF diagram of figure 19. The mineral modes of the Pimampiro pluton plot inside the Tonalite area on the QAPF diagram. According to their IUGS systematics on Igneous Rocks, the distinctive hornblende megacrysts should be reflected on the name of this rock, therefore the rocks from the Pimampiro pluton should be regarded as hornblende tonalite.
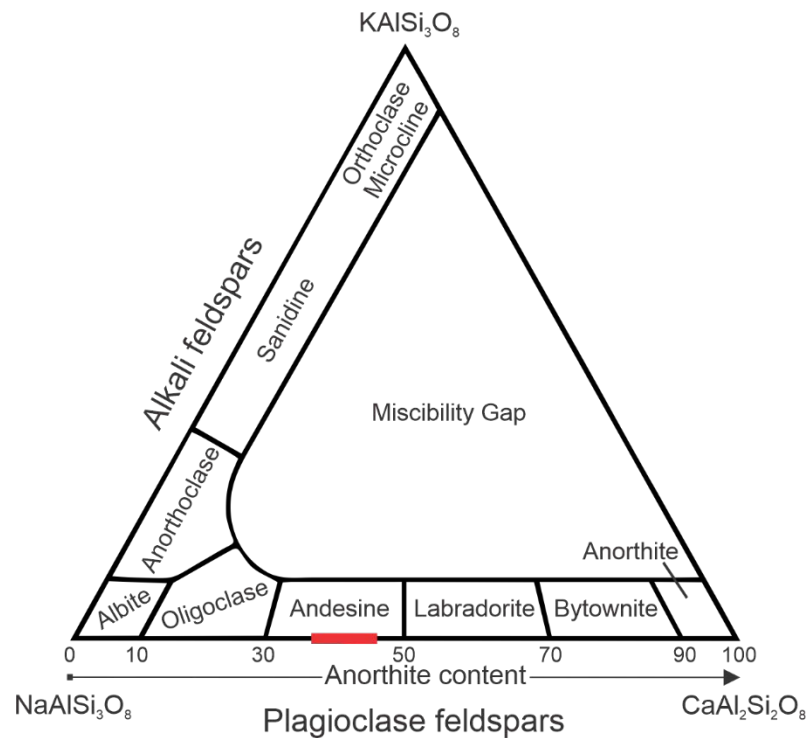
Figure 18. Ternary diagram of feldspar compositions in the Pimampiro pluton. Red bar shows the compositional range of measured plagioclase grains in MOL-01A and MOL-01C. Notice that the plagioclase feldspars can contain up to 10% k-feldspar component.

The predominance of amphiboles as the main mafic facies of the Pimampiro pluton along with the widespread presence of mafic microgranular enclaves relate the Pimampiro pluton tonalite with a mixed origin of crustal and mantle material. The Pimampiro tonalite falls into the Amphibole-bearing Calk-alkaline Granitoids of Barbarin (1999). The features associated with the classification scheme and their presence on the Pimampiro pluton further confirm the utility of this scheme for associating the mineralogy and macroscopic features of igneous bodies with the geodynamic environment in which they formed.
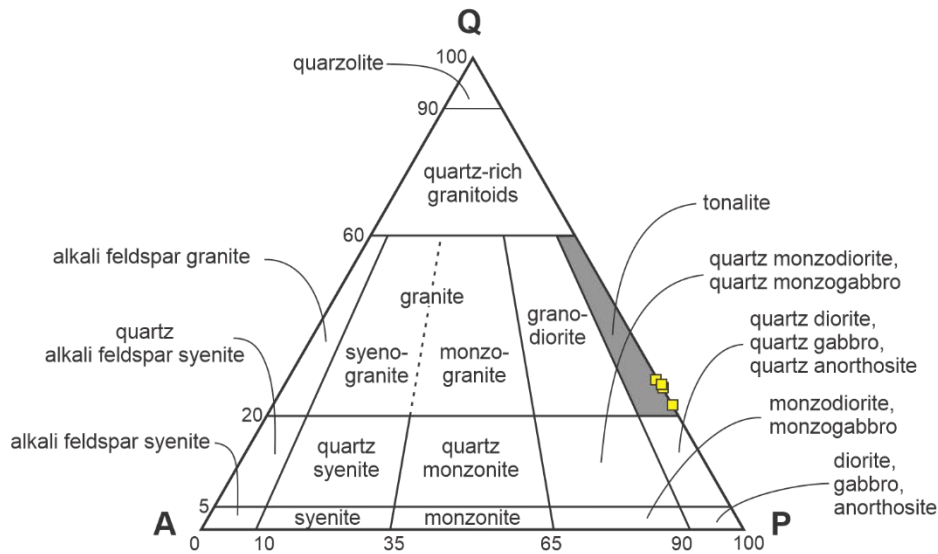
Figure 19. QAP ternary plot for the Pimampiro pluton. The modal percentages (yellow squares) of plagioclase (P= albite + anorthite), quartz (Q) and alkali feldspars (A) obtained from point counting at microscopic level of 4 areas of the Pimampiro pluton thin sections (MOL-01A, MOL-01C). The grey area indicates the corresponding name field for the corresponding classification in the QAPF diagram (Strekeisen, 1974).

5. Discussions

The hydrous nature of the magma forming the Pimampiro pluton is reflected on the high modal percentage of Ca-rich amphibole (35% mode) which most likely reflects the strong influence of water on the formation of the pluton (Vernon, 2014). The high content of hydrated phases is evidence of a water rich melts contributing to the chemistry in which the early crystallization of the amphibole megacrysts occurred.

The megacrystic calcic clinoamphiboles with actinolite cores rimmed by thin subhedral hornblende may suggest long residence times and/or high growth to nucleation rates at the early stages of undercooling of the melt that produced the megacrysts to allow the formation of the large actinolite cores (Marsh, 1988; Vernon, 2014). The presence of small parasitic twins growing on the crystal faces of the hornblende megacrysts in the Pimampiro pluton may suggest that after rapid growth of crystals with diminished nucleation, the nucleation rate increased and thus favored the growth of many small hornblende minerals, some of which nucleated on the low-energy faces of the early megacrysts (Vernon, 2004). The presence of very small anhedral hornblendes in the matrix suggest that rapid cooling occurred at the late stages of emplacement enhancing faster crystallization of the remaining melted portions of the pluton (Marsh, 1988).

The prismatic euhedral cores of plagioclase grains from the Pimampiro pluton and their lobate grain and plagioclase-quartz phase boundaries are analogous to the geometries of plagioclase and quartz leucosomes presented by Berger and Roselle (2001). Based on CSD analyses, they suggest that the growth of the euhedral parts of the plagioclase crystals is controlled by nucleation and growth through cooling, and that the lobate phase boundaries are the product of fast growing against the remaining interstitial space at the late stages of crystallization. According to Velbel (1983), the preferential alteration of plagioclase may be associated with two variables: a) the local chemical composition and b) the orientation of crystal structure with respect to geologic stresses. In the latter case, sericite preferentially pseudomorphing albite twin's lamella would be widespread in thin section (Velbel, 1983). This feature is not observed on the thin sections of the Pimampiro pluton, instead there is a preferential alteration of the cores of zoned grains and mantles of the oscillatory zoned rims (Fig. 9). Sericite alteration also occurs as irregular masses in plagioclase grains with no apparent concentric zoning, instead patchy zoning is commonly observed in these grains. This spatial distribution of sericite alteration in the Pimampiro pluton along with the observed associated plagioclase microtextures may suggests that such alteration is restricted mostly to the Ca-rich components of plagioclase grains. This spatial limitation of sericite alteration in plagioclase of the Pimampiro pluton may suggest a predisposition for An-rich zones (cores and concentric rims) to readily alter in a greater extent than Ab-rich zones in the presence of hydrous acid conditions at the Earth's surface. This hypothesis falls in accordance with the higher weathering rates for high temperature mineral proposed by Goldich (1938) and with the higher anorthite composition near sericitized zones in compositional profiles (Refer to figure 7a-b of Zhang et al., 2014).

The lack of alkali felspars in the Pimampiro pluton and associated microtextures have led to its classification as a tonalite in the scheme of the QAP diagram. Although the exact composition of the altered cores and patchy zoning in plagioclase was not determined, its anorthite composition should be higher than the average composition of unaltered plagioclase (> An45) so that it preferentially weathers to sericite (Goldich, 1938). Although there is not published data on the chemical composition of the Pimampiro pluton, its nature based on its mineralogy can be inferred in terms of the classification presented by Chappell (1974) and Barbarin (1999). The characteristic hornblende-rich mineralogy (hornblende as normative mafic phase) of the Pimampiro pluton as well as the widespread presence of MME suggests it is an I-type granite. Although the distinction between high-potassium and low-potassium calc-alkaline granites cannot be properly done without geochemical analyses, we speculate that the absence of alkali feldspars is indicate of low potassium in the Pimampiro pluton. Following the petrogenetic relationship of Barbarin (1999), the genesis of the Pimampiro pluton is associated with mixing between felsic (crustal) and mafic (mantle) magmas and its characteristics fall on the low-K Amphibole-bearing Calc-alkaline granitoids (ACG). This is in concordance with the geodynamic model presented by Kerr et al. (2002, 2005) for the Late Cretaceous period in which the Pallatanga block was approaching the SAM though an east-dipping subduction zone (Fig. 3).

The presence of widespread MME enclaves suggest that the magmatic chamber that produced the Pimampiro pluton was being refilled by batches of mafic magmas. The lack of marked transitional contacts along the boundaries of the MME and the host rock suggests that mingling and mixing of the magmas occurred, but hybridization was not probably widespread (Vernon, 2004). Following this hypothesis, the enclave-forming mafic magma disaggregated into discrete globules in the felsic host. This process may be reflected by the tear-shaped enclaves in the central parts of the pluton. The felsic magma might have formed by fractionation after melting of mafic or crustal material due to the injection of hot, even more mafic magma into the lower crust (Vernon, 2004), probably associated with subduction-related melting. The pyroxene glomeroporphyritic aggregates of the dike found in the Pimampiro pluton could have been formed by heterogeneous nucleation or synneusis (Vernon, 2004). The former case would imply that the magma was fluid enough to enable the movement of the crystals to produce the glomeroporphyritic texture observed (Vernon, 2018).

6. Conclusions

The Pimampiro pluton is composed by 35% amphibole megacrysts (3 - 5 cm) and phenocrystic amphiboles and biotite (~1 cm average) embedded in a phenocrystic network (65%) of plagioclase feldspar with average Andesine composition (An_{38}-An_{45}) and quartz. Its modal percentages of minerals site these rocks into the Tonalite field of the QAPF diagram. The appropriate name for the Pimampiro pluton rocks based on the IUGS systematics is thus redefined as hornblende-tonalite.

Field evidences show injection of mafic magma into crystallizing felsic host with different stages of interaction through mixing and mingling in the Pimampiro pluton. The presence of oscillatory zoning and sieved texture on the plagioclase cores of the Pimampiro pluton also suggests that these rocks were primarily formed by injections of mafic magma batches into a pre-exiting intermediate magma. The origin of the Pimampiro pluton is then linked to mixing of at least two different magma sources.

The petrogenetic classification of the Pimampiro rock links its mineralogy and enclaves with a subduction-related origin, which is in accordance with the proposed subduction of the Caribbean plateau beneath SAM previous to the collision and accretion of the Pallatanga block as the most probable geodynamic environment for the Late Cretaceous periods in the northern portion of the Cordillera Real of Ecuador.

The Pimampiro pluton in the Cordillera Real is an ellipsoidal tonalitic intrusion containing megacrysts of hornblende hosted and widespread mafic microgranular enclaves. The mineral associations found in the Pimampiro pluton provide a great opportunity to study the processes associated with fractional crystallization and magma mingling and mixing.

7. Bibliography

[a]Aspden, J., Fortey, N., Litherland, M., Viteri, F., & Harrison, S. M. (1992a). Regional S-type granites in the Ecuadorian Andes: Possible remnants of the breakup of western Gondwana. Journal of South American Earth Sciences, 6(3), 123–132. https://doi.org/10.1016/0895-9811(92)90002-G

[b]Aspden, J., Harrison, S. H., & Rundle, C. C. (1992b). New geochronological control for the tectono-magmatic evolution of the metamorphic basement, Cordillera Real and El Oro Province of Ecuador. Journal of South American Earth Sciences, 6(1–2), 77–96. https://doi.org/10.1016/0895-9811(92)90019-U

Aspden, J., & Litherland, M. (1992). The geology and Mesozoic collisional history of the Cordillera Real, Ecuador. Tectonophysics, 205(1–3), 187–204. https://doi.org/10.1016/0040-1951(92)90426-7

Barbarin, B. (1990). Granitoids: Main petrogenetic classifications in relation to origin and tectonic setting. Geological Journal, 25(3-4), 227–238.doi:10.1002/gj.3350250306

Barbarin, B. (1999). A review of the relationships between granitoid types, their origins and their geodynamic environments. Lithos, 46(3), 605–626.doi:10.1016/s0024-4937(98)00085-1

Berger, A., & Roselle, G. (2001). Crystallization processes in migmatites. American mineralogist, 86(3), 215-224.

Bowen, N. L. (1922). The reaction principle in petrogenesis. The Journal of Geology, 30(3), 177-198.

Caricchi, L., Annen, C., Rust, A., and Blundy, J. (2012). Insights into the mechanisms and timescales of pluton assembly from deformation patterns of mafic enclaves. Journal of Geophysical Research, Vol. 117, B11206, Doi:10.1029/2012jb009325.

Carpenter, M. A. (1994). Subsolidus phase relations of the plagioclase feldspar solid solution. In Feldspars and their reactions (pp. 221-269). Springer, Dordrecht.

Chappell, B. W. (1974). Two contrasting granite types. Pacif. Geol., 8, 173-174.

Chappell, B. W., & White, A. J. R. (2001). Two contrasting granite types: 25 years later. Australian Journal of Earth Sciences, 48(4), 489–499.doi:10.1046/j.1440-0952.2001.00882.x

Cherniak, D & Watson, Edward. (2001). Pb Diffusion in zircon. Chemical Geology. 172. 5-24. 10.1016/S0009-2541(00)00233-3.

Chew, D. M., Schaltegger, U., Košler, J., Whitehouse, M. J., Gutjahr, M., Spikings, R. A., & Mišković, A. (2007). U-Pb geochronologic evidence for the evolution of the Gondwanan margin of the north-central Andes. Bulletin of the Geological Society of America, 119(5–6), 697–711. https://doi.org/10.1130/B26080.1

Chicangana, G. (2005). The Romeral fault system: a shear and deformed extinct subduction zone between oceanic and continental lithospheres in northwestern South America. Earth Sciences Research Journal, 9(1), 50–64.

Cochrane, R. (2013). U-Pb thermochronology, geochronology and geochemistry of NW South America: rift to drift transition, active margin dynamics and implications for the volume balance of continents, 191. Retrieved from http://archive-ouverte.unige.ch/unige:30029

Cochrane, R., Spikings, R., Chew, D., Wotzlaw, J. F., Chiaradia, M., Tyrrell, S., et al. (2014a). High temperature (>350°C) thermochronology and mechanisms of Pb loss in apatite. Geochimica et Cosmochimica Acta, 127, 39–56. https://doi.org/10.1016/j.gca.2013.11.028

Cochrane, R., Spikings, R., Gerdes, A., Ulianov, A., Mora, A., Villagómez, D., et al. (2014b). Permo-Triassic anatexis, continental rifting and the disassembly of western Pangaea. Lithos, 190–191, 383–402. https://doi.org/10.1016/j.lithos.2013.12.020

Demange, M. A. (2012). Mineralogy for Petrologists: Optics, Chemistry and Occurrences of Rock-Forming Minerals. CRC Press.

Didier, J., Duthou, J. L., & Lameyre, J. (1982). Mantle and crustal granites: Genetic classification of orogenic granites and the nature of their enclaves. Journal of Volcanology and Geothermal Research, 14(1–2), 125–132. https://doi.org/10.1016/0377-0273(82)90045-2

DiPietro, J. (2013). Landscape Evolution in the United States: Chapter 4 - Mechanisms That Impart Change to Landscapes, Elsevier. ISBN 9780123977991, https://doi.org/10.1016/B978-0-12-397799-1.00004-X.

Egüez, A., & Aspden, J. A. (1993). The Mesozoic-Cenozoic Evolution Of The Ecuadorian Andes.

Goldich, S. S. (1938). A Study in Rock Weathering. Journal of Geology. 46: 17–58. Bibcode:1938JG.....46...17G. doi:10.1086/624619.

Goldsmith, J. R., & Ehlers, E. G. (1952). The Stability Relations of Anorthite and Its Hexagonal Polymorph in the System CaAl2Si2O8-H2O. The Journal of Geology, 60(4), 386-397.

Jaillard, E., Sempere, T., Soler, P., Carlier, G., & Marocco, R. (1995). The role of Tethys in the evolution of the northern Andes between Late Permian and Late Eocene times. 2. The Ocean

Basins and Margins, Volume 8: The Tethys Ocean. https://doi.org/10.1007/978-1-4899-1558-0_15

Kerr, A.C., Aspden, J.A., Tarney, J., Pilatasig, L.F., 2002. The nature and provenance of accreted oceanic blocks in western Ecuador: geochemical and tectonic constraints. J. Geol. Soc. Lond. 159, 577–594.

Kerr, A.C., Tarney, J., 2005. Tectonic evolution of the Caribbean and northwestern South America: the case for accretion of two Late Cretaceous oceanic plateaus. Geology 33, 269–272.

King P. L., Chappell B. W., Allen C. M. & White A. J. R. (2001). Are A-type granites the high-temperature felsic granites? Evidence from fractionated granites of the Wangrah Suite. Australian Journal of Earth Sciences 48, 501–514.

Laves, F. (1952). Phase Relations of the Alkali Feldspars. II. The Stable and Pseudo-Stable Phase Relations in the Alkali Feldspar System. The Journal of Geology, 60(6), 549–574.doi:10.1086/626022

Le Bas, M. J., & Streckeisen, A. L. (1991). The IUGS systematics of igneous rocks. Journal of the Geological Society, 148(5), 825-833.

Le Maitre, R. W., Streckeisen, A., Zanettin, B., Le Bas, M. J., Bonin, B., & Bateman, P. (Eds.). (2005). Igneous rocks: a classification and glossary of terms: recommendations of the International Union of Geological Sciences Subcommission on the Systematics of Igneous Rocks. Cambridge University Press.

Le Maitre, R.W. (1989). A classification of igneous rocks and glossary of terms. Recommendations of the international union of geological sciences subcommission on the systematics of igneous rocks, 193.

Litherland, M. (1994). The Metamorphic belts of Ecuador. Overseas Memoir of the British Geological Survey, 11, 147.

MacKenzie, W. S., & Adams, A. E. (1996). Atlas en color de rocas y minerales en lámina delgada. Elsevier España.

Mark Harrison (1982). Diffusion of 40Ar in hornblende. T. Contr. Mineral. and Petrol. (1982) 78: 324. https://doi.org/10.1007/BF00398927

Marsh, B. D. (1988). Crystal size distribution (CSD) in rocks and the kinetics and dynamics of crystallization. Contributions to Mineralogy and Petrology, 99(3), 277–291. doi:10.1007/bf00375362

Nesse, W. D. (1991). Introduction to optical mineralogy.

Osborn, E. F. (1962). Reaction series for subalkaline igneous rocks based on different oxygen pressure conditions. American Mineralogist; 47 (3-4_Part_1): 211–226.

Pratt, W. T., Duque, P., & Ponce, M. (2005). An autochthonous geological model for the eastern Andes of Ecuador. Tectonophysics, 399(1-4 SPEC. ISS.), 251–278. https://doi.org/10.1016/j.tecto.2004.12.025

Pratt, W., Duque, P., & Ponce, M. (2002). Orthogonal deformation in the eastern Andes of Ecuador. In 5th International Symposium on Andean Geodynamics (ISAG'02), Univ. Toulouse (France) (pp. 485-488).

Raith, M. M., Raase, P. R., & Reinhardt, J. R. (2011). Guide to thin section microscopy. University of Bonn.

Salazar E., Cilio E., Díaz L, (1986). Mapa geológico del Ecuador escala 1:100k Hoja 97: San Gabriel – CT-OII-4095. Dirección General de Geología y Minas (DGGM).

Spikings, R. A., Crowhurst, P. V, & Winkler, W. (2005). (U-Th)/ He - derived thermochronological constraints on the post - middle Miocene tectonic history of the Ecuadorian Andes.

Spikings, R. A., Crowhurst, P. V., Winkler, W., & Villagomez, D. (2010). Syn- and post-accretionary cooling history of the Ecuadorian Andes constrained by their in-situ and detrital thermochronometric record. Journal of South American Earth Sciences, 30(3–4), 121–133. https://doi.org/10.1016/j.jsames.2010.04.002

Spikings, R., Cochrane, R., Villagomez, D., Van der Lelij, R., Vallejo, C., Winkler, W., & Beate, B. (2015). The geological history of northwestern South America: From Pangaea to the early collision of the Caribbean Large Igneous Province (290-75 Ma). Gondwana Research, 27(1), 95–139. https://doi.org/10.1016/j.gr.2014.06.004

Spikings, R., Villagomez, D., Cochrane, R., & Lelij, R. Van Der. (2011). The tectonic history of the Northern Andean Segment (north of 5 ° S) since the Early Triassic: a geochronological and thermochronological study.

Stanley, C. (2017). Lithogeochemical classification of igneous rocks using Streckeisen ternary diagrams. Geochemistry: Exploration, Environment, Analysis, 17(2), 63–91.doi:10.1144/geochem2016-463

Streckeisen, A. (1974). Classification and nomenclature of plutonic rocks recommendations of the IUGS subcommission on the systematics of igneous rocks. Geologische Rundschau, 63(2), 773-786.

Streckeisen, A. (1976). To each plutonic rock its proper name. Earth-Science Reviews, 12(1), 1–33.doi:10.1016/0012-8252(76)90052-0

Tobi, A. C., & Kroll, H. (1975). Optical determination of the An-content of plagioclases twinned by Carlsbad-law; a revised chart. American Journal of Science, 275(6), 731-736.

UNESCO. (2019, April 17). Eleven sites and extensions in Asia, Europe, and South America receive UNESCO Global Geopark Label [Press release]. Retrieved from https://en.unesco.org/news/eleven-sites-and-extensions-asia-europe-and-south-america-receive-unesco-global-geopark-label

Vallejo, C., Spikings, R. A., Horton, B. K., Luzieux, L., Romero, C., Winkler, W., & Thomsen, T. B. (2019). Late cretaceous to miocene stratigraphy and provenance of the coastal forearc and Western Cordillera of Ecuador: Evidence for accretion of a single oceanic plateau fragment. In Andean Tectonics (pp. 209-236). Elsevier.

Velbel, M. A. (1983). A dissolution-reprecipitation mechanism for the pseudomorphous replacement of plagioclase feldspar by clay minerals during weathering. Sciences Géologiques, bulletins et mémoires, 71(1), 139-147.

Vernon, Ron. (2004). A Practical Guide to Rock Microstructure. 10.1017/CBO9780511807206.

Zhang, J.-Y., Ma, C.-Q., Zhang, C., & Li, J.-W. (2014). Fractional crystallization and magma mixing: evidence from porphyritic diorite-granodiorite dykes and mafic microgranular enclaves within the Zhoukoudian pluton, Beijing. Mineralogy and Petrology, 108(6), 777–800. doi:10.1007/s00710-014-0336-4

8. *Figure index*

9. *Abbreviations*

Albite (ab)

Apatite (ap)

Biotite (bt)

Crossed polarized light (XPL)

Epidote (ep)

Feldspar (fsp)

Hornblende (hb)

Magnetite (Mag)

Muscovite (ms)

Orthopyroxene (opx)

Plagioclase (pl)

Plain polarized light (PPL)

Point Counting Method (PCM)

Pyroxene (px)

Quartz (qtz)

Sericite (ser)

South American Margin (SAM)